Available online at www.sciencedirect.com
ScienceDirect
Applied Geochemistry 23 (2008) 203–226
Applied Geochemistry
www.elsevier.com/locate/apgeochem

Dissolved metals and associated constituents in abandoned coal-mine discharges, Pennsylvania, USA. Part 2: Geochemical controls on constituent concentrations

Charles A. Cravotta III

U.S. Geological Survey, 215 Limekiln Road, New Cumberland, PA 17070, United States

Available online 7 October 2007

Abstract

Water-quality data for discharges from 140 abandoned mines in the Anthracite and Bituminous Coalfields of Pennsylvania reveal complex relations among the pH and dissolved solute concentrations that can be explained with geochemical equilibrium models. Observed values of pH ranged from 2.7 to 7.3 in the coal-mine discharges (CMD). Generally, flow rates were smaller and solute concentrations were greater for low-pH CMD samples; pH typically increased with flow rate. Although the frequency distribution of pH was similar for the anthracite and bituminous discharges, the bituminous discharges had smaller median flow rates; greater concentrations of SO_4, Fe, Al, As, Cd, Cu, Ni and Sr; comparable concentrations of Mn, Cd, Zn and Se; and smaller concentrations of Ba and Pb than anthracite discharges with the same pH values. The observed relations between the pH and constituent concentrations can be attributed to (1) dilution of acidic water by near-neutral or alkaline ground water; (2) solubility control of Al, Fe, Mn, Ba and Sr by hydroxide, sulfate, and/or carbonate minerals; and (3) aqueous SO_4-complexation and surface-complexation (adsorption) reactions. The formation of $AlSO_4^+$ and $AlHSO_4^{2+}$ complexes adds to the total dissolved Al concentration at equilibrium with $Al(OH)_3$ and/or Al hydroxysulfate phases and can account for 10–20 times greater concentrations of dissolved Al in SO_4-laden bituminous discharges compared to anthracite discharges at pH of 5. Sulfate complexation can also account for 10–30 times greater concentrations of dissolved Fe^{III} concentrations at equilibrium with $Fe(OH)_3$ and/or schwertmannite ($Fe_8O_8(OH)_{4.5}(SO_4)_{1.75}$) at pH of 3–5. In contrast, lower Ba concentrations in bituminous discharges indicate that elevated SO_4 concentrations in these CMD sources could limit Ba concentrations by the precipitation of barite ($BaSO_4$). Coprecipitation of Sr with barite could limit concentrations of this element. However, concentrations of dissolved Pb, Cu, Cd, Zn, and most other trace cations in CMD samples were orders of magnitude less than equilibrium with sulfate, carbonate, and/or hydroxide minerals. Surface complexation (adsorption) by hydrous ferric oxides (HFO) could account for the decreased concentrations of these divalent cations with increased pH. In contrast, increased concentrations of As and, to a lesser extent, Se with increased pH could result from the adsorption of these oxyanions by HFO at low pH and desorption at near-neutral pH. Hence, the solute concentrations in CMD and the purity of associated "ochres" formed in CMD settings are expected to vary with pH and aqueous SO_4 concentration, with potential for elevated SO_4, As and Se in ochres formed at low pH and elevated Cu, Cd, Pb and Zn in ochres formed at near-neutral pH. Elevated SO_4 content of ochres could enhance the adsorption of cations at low pH, but decrease the adsorption of anions such as As. Such information on environmental processes that control element concentrations in aqueous samples and associated precipitates could be useful in

E-mail address: cravotta@usgs.gov

0883-2927/$ - see front matter Published by Elsevier Ltd.
doi:10.1016/j.apgeochem.2007.10.003

the design of systems to reduce dissolved contaminant concentrations and/or to recover potentially valuable constituents in mine effluents.
Published by Elsevier Ltd.

1. Introduction

Abandoned coal-mine discharges (CMD) can be corrosive or encrusting and can impair aquatic habitat, water-delivery systems, bridges, and associated infrastructure (Barnes and Clarke, 1969; Winland et al., 1991; Earle and Callaghan, 1998; Bigham and Nordstrom, 2000; Houben, 2003). Although dissolved SO_4, Fe, Al, and Mn are widely recognized as mineral constituents of concern, numerous trace metals have also been documented in CMD, particularly in strongly acidic, low-pH solutions (Hyman and Watzlaf, 1997; Rose and Cravotta, 1998; Nordstrom and Alpers, 1999; Nordstrom, 2000; Nordstrom et al., 2000; Cravotta, 2008). The dissolved metals and associated constituents in CMD can be toxic to aquatic and terrestrial organisms. Generally, the toxicity of a dissolved element increases with its concentration after nutritional requirements, if any, are met (Smith and Huyck, 1999).

The pH of a solution is an important measure for evaluating aquatic toxicity and corrosiveness. The severity of toxicity or corrosion tends to be greater under low-pH or high-pH conditions than at near-neutral pH, because the solubility of many metals can be described as amphoteric, with a greater tendency to dissolve as cations at low pH or anionic species at high pH (Langmuir, 1997). For example, Al hydroxide and aluminosilicate minerals have their minimum solubility at pH 6–7 (Nordstrom and Ball, 1986; Bigham and Nordstrom, 2000), and brief exposure to relatively low concentrations of dissolved Al can be toxic to fish and other aquatic organisms (Baker and Schofield, 1982; Elder, 1988). Accordingly, the U.S. Environmental Protection Agency (2000, 2002a,b) recommends pH 6.5–9.0 for protection of freshwater aquatic life and pH 6.5–8.5 for public drinking supplies. Nevertheless, pH is not the sole determinant of metals solubility.

Anions including SO_4^{2-}, HCO_3^- and, less commonly, Cl^- can be elevated above background concentrations in CMD (Cravotta, 2008), and polyvalent cations such as Al^{3+} and Fe^{3+} tend to associate with such ions of opposite charge (Ball and Nordstrom, 1991; Nordstrom, 2004). Ion-pair formation, or aqueous-complexation reactions, between dissolved cations and anions can increase the total concentration of metals in a solution at equilibrium with a mineral and can affect the bioavailability and toxicity of metal ions in aquatic ecosystems (e.g. Rose et al., 1979; Langmuir, 1997; Sparks, 2005). Eventually, the solutions can become saturated, or reach equilibrium, with respect to various sulfate, carbonate, or hydroxide minerals that establish limits for the dissolved metal concentrations.

Dissolved trace elements, such as Pb and Cu, in natural waters can be limited to concentrations lower than expected on the basis of trace-mineral solubility because of surface complexation, or adsorption, of the elements onto solid surfaces (Rose et al., 1979). Hydrous Fe^{III}, Al, and $Mn^{III–IV}$ oxides that precipitate in oxidizing CMD environments are important sorbents because of their large surface areas, tendencies to form colloids and to coat other geological materials, and potential for the oxide surfaces to have variable electrostatic charges (Hem, 1977, 1978, 1985; Loganathan and Burau, 1973; McKenzie, 1980; Davis and Kent, 1990; Kooner, 1993; Coston et al., 1995; Langmuir, 1997; Webster et al., 1998; Kairies et al., 2005; Sparks, 2005). Surface hydroxyl groups at the solution interface tend to dissociate at high pH or to protonate at low pH, giving rise to a negative or positive surface charge, respectively. Cations, such as Cd, Cu, Pb, Ni and Zn, tend to be adsorbed by the negatively charged oxide surfaces at near-neutral pH, whereas oxyanions, such as sulfate, arsenate, arsenite, selenate, selenite and borate, tend to be adsorbed by the positively charged surfaces at lower pH (Dzombak and Morel, 1990; Davis and Kent, 1990; Stumm and Morgan, 1996; Drever, 1997; Langmuir, 1997). These conditions for adsorption are consistent with reported enrichment of CMD ochres and streambed coatings with Cd, Cu, Pb, Ni and Zn at near-neutral pH and with S and As at low pH (Winland et al., 1991; Hedin et al., 1994; Rose and Ghazi, 1997; Cravotta and Trahan, 1999; Cravotta and Bilger, 2001; Cravotta et al., 2001; Hedin, 2003; Kairies et al., 2005; Cravotta, 2005, 2008).

This report examines relationships between pH, SO_4, and metal concentrations in CMD samples

from abandoned coal mines in the Bituminous and Anthracite Coalfields of Pennsylvania. Similarities and differences in the flow rate and chemistry between the anthracite and bituminous CMD samples are examined. The potential formation of aqueous complexes, surface complexes, and stability of possible solid phases in contact with aqueous solutions are evaluated with respect to thermodynamic equilibrium at near-surface temperature and pressure conditions. Additionally, ratios of Br/Cl are used to evaluate potential for mixing of fresh ground water with road salts or deep brine. A companion report by Cravotta (2008) describes the chemical and hydrological data in more detail and examines the correlations between flow rate, pH, constituent concentrations, and constituent loadings.

2. Methods of sampling and analysis

The study area description, a map showing the sampling locations, and details on the site characteristics and methods of data collection and chemical analysis are given in the companion report by Cravotta (2008). Essential information on sampling and analytical methods is summarized below.

2.1. Water-quality sampling and analysis

In summer and fall 1999, water-quality samples from 140 abandoned, discharging coal mines in the Anthracite and Bituminous Coalfields of Pennsylvania were collected by the U.S. Geological Survey (USGS) for analysis of chemical concentrations and loading. The 140 discharges, including 99 from bituminous mines and 41 from anthracite mines, were selected among thousands of CMD sources statewide based on their geographic distribution, accessibility, and potential for substantial loadings of dissolved metals. Most of the sampled discharges were from underground mines. All the CMD sources were discharging by gravity when sampled. Flow was measured at each site by use of a current meter or bucket and stopwatch.

To minimize effects from aeration, electrodes were immersed and samples were collected as close as possible to the point of discharge. Field data for flow rate, temperature, specific conductance (SC), dissolved O_2 (DO), pH and redox potential (Eh) were measured at each site when samples were collected in accordance with standard methods (Rantz et al., 1982a,b; Wood, 1976; U.S. Geological Survey, variously dated; Ficklin and Mosier, 1999). All meters were calibrated in the field using electrodes and standards that had been thermally equilibrated to sample temperatures. Field pH and Eh were determined using a combination Pt and Ag/AgCl electrode with a pH sensor. The electrode was calibrated in pH 2.0, 4.0 and 7.0 buffer solutions and in ZoBell's solution (Wood, 1976; U.S. Geological Survey, variously dated). Values for Eh were corrected to 25 °C relative to the standard hydrogen electrode in accordance with methods of Wood (1976) and Nordstrom (1977).

An unfiltered subsample for analysis of alkalinity was capped leaving no head space and stored on ice. Alkalinity was analyzed in the laboratory within 48 h of sampling by titration with H_2SO_4 to the endpoint pH of 4.5 (American Public Health Association, 1998; Kirby and Cravotta, 2005a,b). The pH before and during alkalinity titrations was measured using a liquid-filled combination Ag/AgCl pH electrode calibrated in pH 4.0, 7.0, and 10.0 buffer solutions. The net acidity of the CMD samples was computed from field pH, alkalinity and dissolved Fe, Mn, and Al concentrations (Kirby and Cravotta, 2005b; Cravotta, 2008).

Subsamples for analysis of "dissolved" constituents were filtered through a 0.45-μm pore-size nitrocellulose capsule filter using the clean-sampling methods of Horowitz et al. (1994). Although colloidal particles could pass through 0.45-μm pore-size filters, constituent concentrations in the filtered samples are interpreted hereinafter as dissolved solutes. The subsample for cation analyses was preserved with trace-element grade HNO_3 to pH < 2. Anions (SO_4, Cl, F, NO_3, NO_2 and PO_4) in filtered, refrigerated samples were analyzed by ion chromatography (IC) (Fishman and Friedman, 1989; Crock et al., 1999). Concentrations of major cations and trace metals in the filtered, acidified samples were determined using inductively coupled plasma optical emission spectroscopy (ICP-OES) and inductively coupled plasma mass spectrometry (ICP-MS) (Fishman and Friedman, 1989; Crock et al., 1999). Results for replicate analyses were averaged before evaluation. When values for one or more replicates were reported as not detected, the lowest reported value or the lowest non-detect value was used as the result.

2.2. Computation of aqueous complexation and mineral saturation

Activities of aqueous species, partial pressure of CO_2 (P_{CO_2}), and mineral-saturation index (SI)

values were calculated using the WATEQ4F version 2.63 computer program (Ball and Nordstrom, 1991). The activities of Fe^{II} and Fe^{III} species were computed on the basis of the measured Eh, Fe concentration, and temperature of the samples. Nordstrom (1977) and Nordstrom et al. (1979) have shown there is good agreement between the measured Eh and that predicted by the Fe^{II}/Fe^{III} couple in acidic mine waters. For the 90 samples that had alkalinity > 0, the P_{CO_2} was computed on the basis of measured pH, alkalinity, and temperature. Computed SI values for silicate, oxide, carbonate and sulfate minerals that could be present in coal deposits or associated wall rocks or that may form as solutions oxidized or evaporated at the land surface were summarized as a function of pH.

Stability diagrams were developed to evaluate the potential for equilibrium of specific elements (Ca, Mg, Al, Fe, Mn, Ba, Cd, Cu, Pb, Sr, Zn) with respect to hydroxide, sulfate and carbonate minerals (solubility) for specified ranges of pH, Eh, P_{CO_2}, SO_4 and Cl. The theoretical stability boundaries for minerals and aqueous species computed with spreadsheet models were plotted as reference lines or curves on "pC–pH" and "Eh–pH" diagrams (e.g. Snoeyink and Jenkins, 1981; Drever, 1997; Langmuir, 1997). Then, data on sample pH, Eh, or activities of uncomplexed cations (Al^{3+}, Fe^{3+}, Fe^{2+}) and major aqueous complexes computed with WATEQ4F were plotted as points on the stability diagrams. Reactions and associated equilibrium constants for relevant species and solids in the spreadsheet models were obtained mostly from the WATEQ4F thermodynamic database (Nordstrom et al., 1990; Ball and Nordstrom, 1991; Drever, 1997) and supplemented with other data for Fe^{III} minerals (Bigham et al., 1996; Yu et al., 1999). Thermodynamic data that were used are summarized in the Appendix (Tables A1–A3). Equilibrium reactions and associated thermodynamic data for hydroxide, sulfate, and carbonate minerals and aqueous species involving SO_4, CO_3, Fe^{III} and Al are given in Table A1. Speciation and solubility data for Al, Ba, Ca, Cd, Co, Cu, Fe^{II}, Fe^{III}, Mg, Mn^{II}, Ni, Pb^{II}, Sr and Zn are summarized in Table A2; detailed reactions for Pb^{II} with data from Table A2 are provided as an example in Table A3.

2.3. Computation of surface complexation

Adsorption and desorption, or surface complexation, of cations and anions on hydrous ferric hydroxide (HFO) particles were evaluated using a diffuse double-layer modeling approach with PHREEQC (Parkhurst and Appelo, 1999), surface-complexation data from Dzombak and Morel (1990), and aqueous speciation data from Ball and Nordstrom (1991). Although the concentrations of dissolved solutes in the models could be specified based on the known ranges for the CMD samples, knowledge of the amounts and properties of the sorbent HFO was lacking. Models were developed for different cations and anions by first modifying an example for Zn adsorption on HFO ("example 8" of Parkhurst and Appelo, 1999) that implicitly specified the HFO surface assemblage in equilibrium with a solution of fixed composition. The HFO solid was specified as 0.09 g kg^{-1} solution, with a specific surface area of 600 m^2 g^{-1} consisting of 5×10^{-6} moles of strong binding sites and 2×10^{-4} moles of weak binding sites. With data from Dzombak and Morel (1990), additional sorbate elements were considered (cations: Ba, Ca, Cd, Co, Cu, Mn^{II}, Ni, Pb^{II}, Sr; anions: As, B, Cr, Se, S, V). Aqueous speciation and adsorption distribution were computed for a constant concentration of the sorbate element and a range of pH values. Plots were created to summarize the percentage of the sorbate element distributed between the solution and sorbent as a function of pH. The models developed for anion adsorption simulated a NaCl background matrix, whereas those for cation adsorption also specified initial concentrations of SO_4^{2-} and HCO_3^- to identify effects of metal complexes with OH^-, Cl^-, SO_4^{2-} and CO_3^{2-} species.

3. Results – characteristics of anthracite and bituminous CMD samples

Data on the flow rates, pH, acidity, alkalinity and selected solute concentrations for the 140 CMD samples collected in 1999 from abandoned coal mines in the Anthracite and Bituminous Coalfields of Pennsylvania are summarized in Table 1 and Figs. 1 and 2. Sampled flow rates at the 140 CMD sites ranged from 0.028 to 2.210 L s^{-1}. The anthracite discharges had greater median flow rates than the bituminous discharges (Table 1). Furthermore, median and maximum flow rates for the anthracite mine discharges generally exceeded those for the bituminous mines for the same pH class interval (Fig. 1).

Generally, flow rate and alkalinity increased with pH, whereas acidity, SO_4 and metal concentrations

Table 1
Summary of hydrochemical characteristics of discharges from 140 abandoned coal mines in Pennsylvania, 1999[a]

Coalfield and number of samples	Flow rate ($L\ s^{-1}$)	Temperature (°C)	Specific ($\mu S\ cm^{-1}$)	Redox potential, Eh (mV)	pH, field	Alkalinity ($mg\ L^{-1}$ as $CaCO_3$)	Net acidity[b] ($mg\ L^{-1}$ as $CaCO_3$)	Hardness[c] ($mg\ L^{-1}$ as $CaCO_3$)	Sulfate, SO_4 ($mg\ L^{-1}$)
Anthracite $N = 41$	64.0 (0.028; 2.21)	11.4 (8.8; 26.6)	692 (131; 2050)	390 (170; 770)	5.1 (3.0; 6.3)	3 (0; 120)	43 (−79; 588)	244 (23; 770)	260 (34; 1300)
Bituminous $N = 99$	12.5 (0.227; 278)	12.0 (9.0; 16.5)	1480 (495; 3980)	390 (140; 800)	5.2 (2.7; 7.3)	14 (0; 510)	76 (−326; 1587)	433 (117; 1811)	580 (120; 2000)
	Calcium, Ca ($mg\ L^{-1}$)	Magnesium, Mg ($mg\ L^{-1}$)	Sodium, Na ($mg\ L^{-1}$)	Potassium, K ($mg\ L^{-1}$)	Chloride, Cl ($mg\ L^{-1}$)	Silica, SiO_2 ($mg\ L^{-1}$)	Aluminum, Al ($mg\ L^{-1}$)	Iron, Fe ($mg\ L^{-1}$)	Manganese, Mn ($mg\ L^{-1}$)
Anthracite $N = 41$	37 (3.3; 180)	35 (3.6; 87)	6.1 (0.69; 67)	1.8 (0.7; 3.9)	6.3 (0.1; 110)	13 (5.8; 51)	0.28 (0.007; 26)	15 (0.046; 312)	2.9 (0.019; 19)
Bituminous $N = 99$	110 (19; 410)	38 (8.5; 210)	23 (1.0; 500)	3.3 (0.5; 12)	7.7 (0.4; 460)	19 (8.2; 67)	1.5 (0.008; 108)	43 (0.16; 512)	2.3 (0.12; 74)
	Arsenic, As ($\mu g\ L^{-1}$)	Barium, Ba ($\mu g\ L^{-1}$)	Cadmium, Cd ($\mu g\ L^{-1}$)	Copper, Cu ($\mu g\ L^{-1}$)	Lead, Pb ($\mu g\ L^{-1}$)	Nickel, Ni ($\mu g\ L^{-1}$)	Selenium, Se ($\mu g\ L^{-1}$)	Strontium, Sr ($\mu g\ L^{-1}$)	Zinc, Zn ($\mu g\ L^{-1}$)
Anthracite $N = 41$	0.62 (<0.03; 15)	18 (13; 31)	0.12 (<0.01; 2.1)	0.85 (0.4; 91)	0.68 (<0.05; 11)	83 (19; 620)	0.4 (<0.2; 3.9)	190 (27; 2700)	130 (3.0; 1000)
Bituminous $N = 99$	2.0 (0.1; 64)	13 (2.0; 39)	0.12 (<0.01; 16)	2.2 (0.4; 190)	0.10 (<0.05; 4.6)	90 (2.6; 3200)	0.6 (<0.2; 7.6)	1000 (47; 3600)	140 (0.6; 10,000)

[a] Median (minimum; maximum); $L\ s^{-1}$, liters per second; °C, degrees Celsius; $\mu S\ cm^{-1}$, microsiemens per centimeter; mV, millivolts; $mg\ L^{-1}$, milligrams per liter; $\mu g\ L^{-1}$, micrograms per liter. Sample site locations shown in Fig. 1 of Cravotta (2008). Detailed data available from Cravotta (2008).

[b] Net acidity = (acidity, computed − Alkalinity, measured) per Kirby and Cravotta (2005b). Acidity, computed ($mg\ L^{-1}$ $CaCO_3$) $= 50 \cdot (10^{(3-pH)} + 3 \cdot C_{Al}/26.98 + 2 \cdot C_{Fe}/55.85 + 2 \cdot C_{Mn}/54.94)$, where C_{Al}, C_{Fe}, and C_{Mn} are dissolved aluminum, iron, and manganese concentration, respectively, in milligrams per liter.

[c] Hardness ($mg\ L^{-1}$ $CaCO_3$) $= 2.5 \cdot C_{Ca} + 4.1 \cdot C_{Mg}$, where C_{Ca} and C_{Mg} are dissolved calcium and magnesium concentration, respectively, in milligrams per liter.

decreased (Fig. 1). These trends imply (1) neutralization of CMD did not result solely by mineral dissolution but also involved dilution of initially acidic water by alkaline ground water or surface water or (2) decreased pyrite oxidation because of decreased contact time with increased flows. Regardless of the cause, mines with large flows tended to be less acidic and have greater pH than those with small flows. Larger flow rates for anthracite discharges than bituminous discharges reflect differences in the physiographic and geologic settings between the two coalfields (Berg et al., 1989; Edmunds, 1999; Eggleston et al., 1999) and indicate that, on average, the anthracite mines have larger recharge areas and more extensive flooded volumes compared to the bituminous mines. Because anthracite mine complexes historically connected multiple coalbeds and extended beneath valleys to hundreds of meters below the regional water table, their mined areas and associated discharge volumes tend to be substantially greater than those from contemporaneous surface mines or bituminous mines that access one or two coalbeds within isolated hilltops.

The field pH of the 140 CMD samples ranged from 2.7 to 7.3, with the majority either acidic (pH 2.5–4) or near neutral (pH 6–7) (Table 1, Fig. 1). This bimodal frequency distribution of pH for the CMD samples was discussed in detail by Cravotta et al. (1999) and Kirby and Cravotta (2005a,b). Although the minimum and maximum pH values were associated with bituminous mine discharges, the median pH values of 5.1 and 5.2 were similar for the 41 anthracite and 99 bituminous discharges, respectively (Table 1).

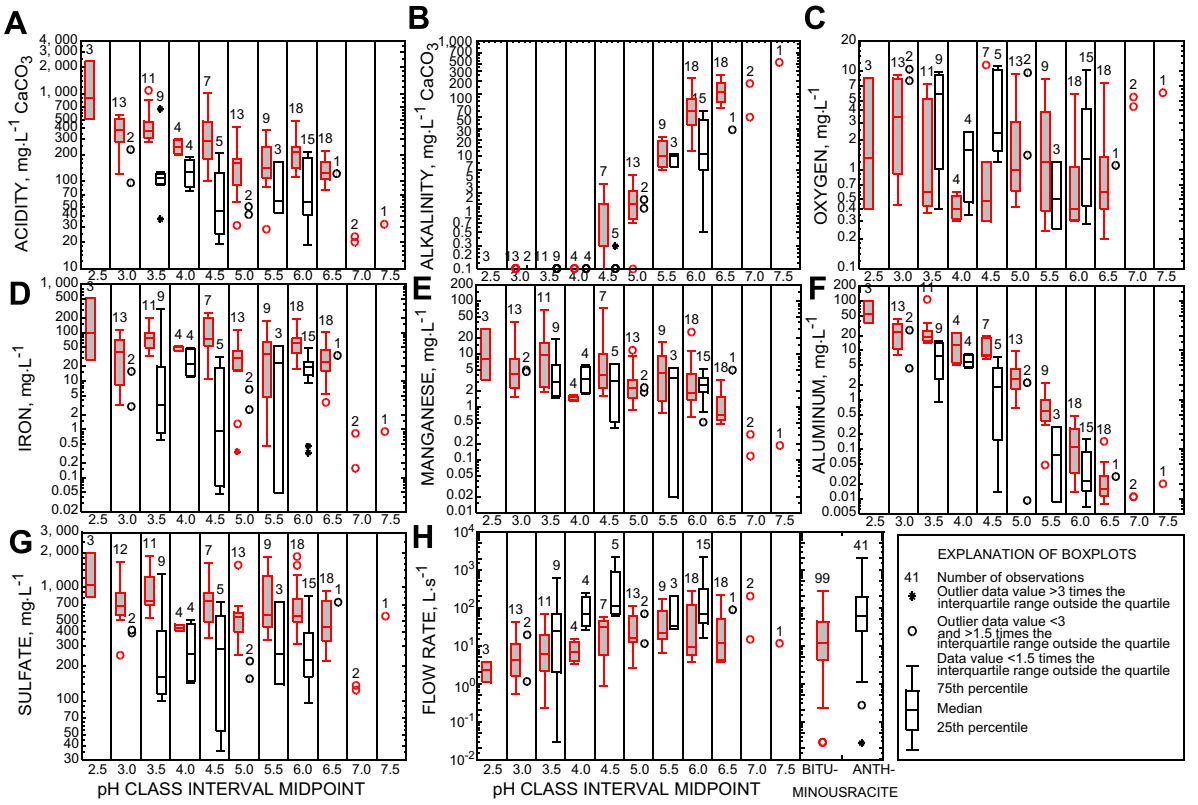

Fig. 1. Boxplots showing concentrations of acidity, alkalinity, associated solutes, and flow compared to pH of 140 abandoned mine discharges in Pennsylvania, 1999: (A) computed acidity; (B) alkalinity; (C) oxygen; (D) Fe; (E) Mn; (F) Al; (G) SO_4; (H) flow. Shaded box, bituminous; open box, anthracite.

Alkalinity concentrations ranged from 0 ($pH \leqslant 4.4$; 50 samples) to 510 mg L^{-1} as $CaCO_3$ (Table 1). Computed net acidity concentrations, which exclude contributions from dissolved CO_2, ranged from −326 to 1587 mg L^{-1} as $CaCO_3$ (Table 1). Concentrations of dissolved SO_4 (34–2000 mg L^{-1}), Fe (0.046–512 mg L^{-1}), Al (0.007–108 mg L^{-1}) and Mn (0.019–74 mg L^{-1}) varied significantly (Table 1). Generally, the highest concentrations of acidity, SO_4, Fe, Al, Mn and most other metals were associated with low-pH samples. Although a few samples were saturated with DO (10–12 mg L^{-1}), median concentrations of DO generally were low (<2 mg L^{-1}) throughout the range of pH (Fig. 1), consistent with the predominance of dissolved Fe^{II} and Mn^{II} species in most CMD samples.

The bituminous discharges generally contained greater concentrations of total dissolved solids than the anthracite discharges as a whole (Table 1) or with the same pH values (Figs. 1 and 2) as indicated by greater median and maximum values for specific conductance and concentrations of alkalinity, acidity, hardness, SO_4, Fe, Al, Mn, and other solutes, including Cd, Cu, Ni, Sr and Zn. In contrast, the median concentrations of dissolved Ba and Pb in bituminous discharges were less than those for the anthracite discharges (Table 1, Fig. 2). As noted above, relatively low concentrations of dissolved mineral constituents in the anthracite discharges could result from dilution of initially acidic CMD with a freshwater source containing limited dissolved solids. Such dilution could affect aqueous speciation and mineral solubilities.

4. Discussion – geochemical controls on constituent concentrations

The widespread occurrence of SO_4, Fe, Mn, Al, As, Ba, Cd, Cu, Pb, Ni, Se, Sr and Zn in CMD samples (Figs. 1 and 2) results from the mobilization of these constituents by the weathering of pyrite and associated minerals in coal and surrounding sedimentary wall rocks. Under oxidizing conditions, pyrite oxidation produces H_2SO_4 that reacts with carbon-

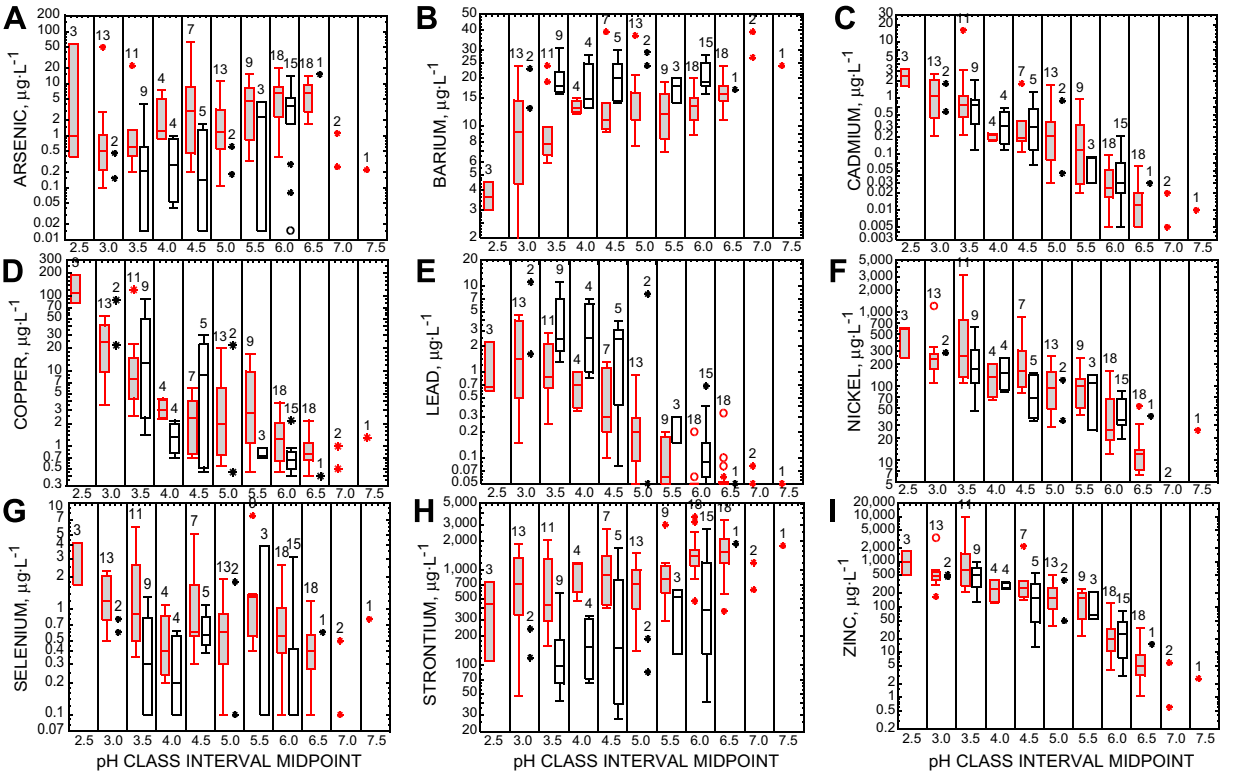

Fig. 2. Boxplots showing concentrations of selected trace elements as a function of pH for 140 abandoned mine discharges in Pennsylvania, 1999: (A) As; (B) Ba; (C) Cd; (D) Cu; (E) Pb; (F) Ni; (G) Se; (H) Sr; (I) Zn. Shaded box, bituminous; open box, anthracite.

ate, silicate and oxide minerals along pathways downflow from the pyrite (e.g. Cravotta, 1994; Blowes and Ptacek, 1994). Generally, the pH, alkalinity, and concentrations of alkali and alkaline earth cations increase because of the wall rock reactions, whereas SO_4 concentrations remain constant. On the other hand, reducing conditions also can lead to increased pH but with corresponding decreases in the concentrations of SO_4 and certain metals (Stumm and Morgan, 1996; Drever, 1997; Langmuir, 1997). Hence, concentrations of dissolved metals and other trace constituents can increase or decrease as the CMD approaches neutrality. Such variations in solute concentrations can be explained by geochemical processes including oxidation and reduction, mineral dissolution and precipitation, aqueous-complexation, and surface-complexation (adsorption and desorption) reactions.

4.1. Aqueous complexation and mineral solubility controls of constituents in CMD samples

Although Fe^{III} and Al hydroxide minerals are insoluble at near-neutral pH, most divalent cations, including Fe^{II}, Mn, Cu, Cd, Pb and Zn, form relatively soluble hydroxides (Fig. 3). Precipitation of Cu^{II}, Fe^{II}, and other divalent metal hydroxides generally will not limit the dissolved metal concentrations until solutions become highly alkaline (pH > 9). Furthermore, as demonstrated later, aqueous complexation with SO_4^{2-}, CO_3^{2-}, HCO_3^-, Cl^-, and/or other anions can increase the dissolved metal concentration at equilibrium with its hydroxide. Nevertheless, observed concentrations of dissolved Fe^{II}, Cu, Cd, Pb, Zn, and other trace metals tend to be substantially lower than these solubility limits. Within the pH range of CMD, many trace metals can be adsorbed by hydrous Fe^{III}, Al and Mn^{IV} oxides (e.g. Dzombak and Morel, 1990; Davis and Kent, 1990; Kooner, 1993; Coston et al., 1995; Webster et al., 1998) and/or precipitate as sulfate or carbonate minerals. Although most trace metals are capable of forming pure sulfate or carbonate phases, Cd, Cu, Pb, Zn, Ba and Sr commonly substitute for Ca, Mg and Fe in calcite ($CaCO_3$), aragonite ($CaCO_3$), dolomite ($CaMg(CO_3)_2$), ankerite ($Ca(Fe,Mg)(CO_3)_2$) and siderite ($FeCO_3$) (Hanshaw and Back, 1979; Veizer, 1983; Mozley, 1989).

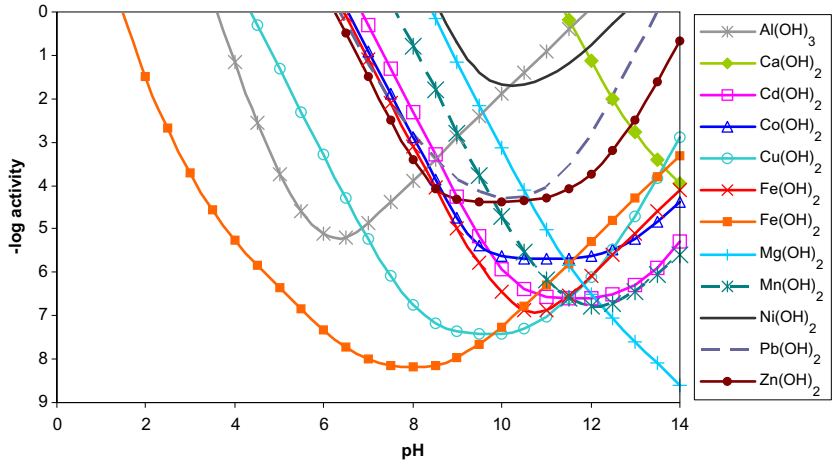

Fig. 3. Solubilities of various metal hydroxide compounds as a function of pH at 25 °C. Thermodynamic data are summarized in Table A2. Solubility computations considered only pH and formation of hydroxyl species.

Barium and Sr can substitute for Ca in gypsum ($CaSO_4 \cdot 2H_2O$) and for one another in barite ($BaSO_4$) and celestite ($SrSO_4$) (Hanor, 1968). Furthermore, As, Cu, Cd, Pb, Zn, and other trace elements can be impurities in pyrite or form other less abundant sulfide minerals (e.g. Hammarstrom and Smith, 2002; Hammarstrom et al., 2006). Consequently, trace-element concentrations tend to be controlled by reactions with various minerals in conjunction with aqueous and surface complexation.

The relations between the pH and concentrations of major and trace elements in CMD samples varied among the constituents (Figs. 1 and 2), implying different origins or mechanisms could control the element concentrations. Acidity and dissolved Al, Cd, Cu, Pb, Ni, Zn and, to a lesser extent, SO_4, Mn and Se concentrations were inversely correlated with pH of the CMD (Figs. 1 and 2). An inverse correlation between the constituent concentration and pH implies greater rate of release of the constituents or greater solubility at low pH than at near-neutral pH. In contrast, alkalinity, As, Ba and Sr concentrations were positively correlated with pH, whereas Fe and Ca concentrations were not correlated with pH. A positive correlation with pH could result from desorption (As) or release of a constituent during neutralization reactions with calcareous solids (Ba, Sr). The lack of correlation between pH and dissolved Fe or Ca is consistent with a high solubility for secondary compounds with these elements over a wide range of pH (Fe^{II}, Ca).

The CMD samples had elevated P_{CO_2} values ($10^{-2.45}$–$10^{-0.54}$ atm.) compared to atmospheric P_{CO_2} of $10^{-3.5}$ atm., and were mostly undersaturated with carbonate minerals (Fig. 4). The median P_{CO_2} was $10^{-1.0}$ atm. Although some samples with near-neutral pH and elevated alkalinity approached saturation with calcite, siderite and rhodochrosite ($MnCO_3$), all were undersaturated with dolomite, smithsonite ($ZnCO_3$), cerrusite ($PbCO_3$) and witherite ($BaCO_3$) (Fig. 4). The CMD samples with highest pH and alkalinities were near saturation, but not supersaturated, with calcite; these samples had some of the highest Na concentrations. Such Na-HCO_3–SO_4 waters could acquire Na by Ca ion exchange (Foster, 1950; Cravotta et al., 1994). For such instances, where Ca is removed from solution, calcite could become undersaturated despite elevated pH and alkalinity.

The CMD samples commonly were saturated with barite but were undersaturated with most other sulfate minerals (Fig. 4). Although SI values for gypsum approached saturation (−3.1 to −0.1), those for melanterite ($FeSO_4 \cdot 7H_2O$), zincosite ($ZnSO_4$), anglesite ($PbSO_4$) and celestite were far below saturation. These results indicate that if the CMD encounters gypsum or other sulfates, the constituent elements could be mobilized as aqueous species. Nevertheless, the presence of SO_4 could enhance precipitation of Ba, Al, and Fe^{III}, as discussed below.

Dissolved Al and SO_4 concentrations typically were elevated for the low-pH CMD samples, mainly from bituminous mines (Fig. 1). Computed SI values indicated the CMD samples with pH < 4 were undersaturated, whereas those with pH > 5 were saturated with various aluminosilicate or Al hydroxysulfate

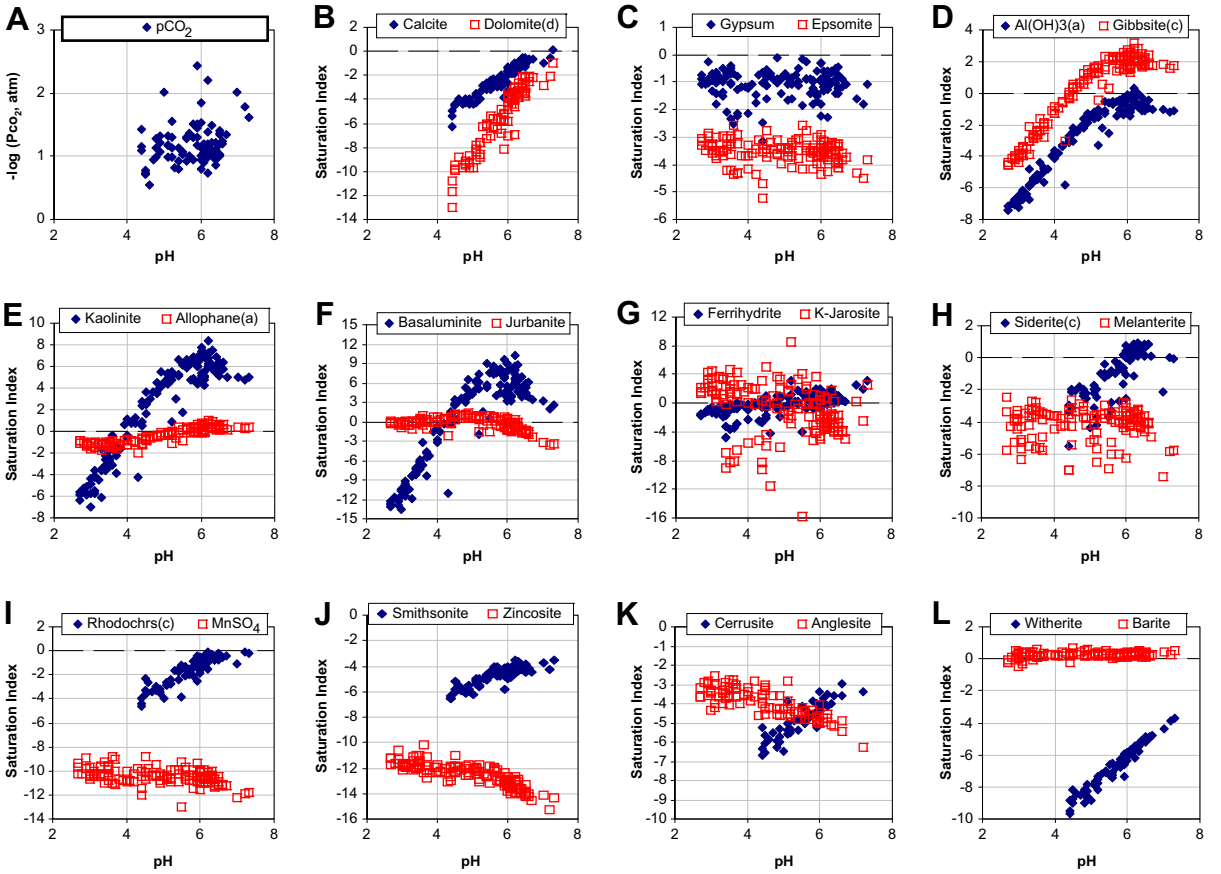

Fig. 4. Partial pressure of CO_2 and saturation indices for minerals and other solids computed with WATEQ4F (Ball and Nordstrom, 1991) as a function of pH of 140 abandoned mine discharges in Pennsylvania, 1999: (A) partial pressure of CO_2; (B) calcite and dolomite; (C) gypsum and epsomite; (D) amorphous $Al(OH)_3$ and gibbsite; (E) kaolinite and allophane; (F) basaluminite and jurbanite; (G) ferrihydrite and jarosite; (H) siderite and melanterite; (I) rhodochrosite and $MnSO_4$; (J) smithsonite and zincosite; (K) cerrusite and anglesite; (L) witherite and barite. Solids, as identified in WATEQ4F, have parenthetical letters indicating: (a), amorphous; (c), crystalline; (d), disordered.

minerals (Fig. 4), including kaolinite ($Al_2Si_2O_5(OH)_4$), illite ($K_{0.6}Mg_{0.25}Al_{2.3}Si_{3.5}O_{10}(OH)_2$), chlorite ($Mg_5Al_2Si_3O_{10}(OH)_8$), allophane ($[Al(OH)_3]_{(1-x)}[SiO_2]_{(x)}$ where $x = 1.24$–0.135 pH), gibbsite ($Al(OH)_3$), amorphous $Al(OH)_3$, basaluminite ($Al_4(OH)_{10}(SO_4)$) and alunite ($KAl_3(SO_4)_2(OH)_6$). Hence, aluminosilicates in shale associated with anthracite and bituminous coal deposits (e.g. Cravotta, 1994; Cravotta et al., 1994) could be sources of dissolved Al in the low-pH CMD samples, and Al hydroxides or hydroxysulfates could limit concentrations of dissolved Al in the near-neutral pH samples.

The general decline in dissolved Al concentration with increased pH and greater concentrations of dissolved Al in bituminous discharges are consistent with solubility control by Al hydroxide and/or hydroxysulfate minerals and the formation of $AlSO_4$ complexes (Fig. 5A and B). The concentration of dissolved Al at equilibrium with solid $Al(OH)_3$ will increase with increased concentration of SO_4 due to formation of $AlSO_4$ complexes, particularly at pH < 5. Speciation computations demonstrate that the formation of $AlSO_4^+$ and $AlHSO_4^{2+}$ could increase the solubility, or total concentration, of Al. For example, adding 2000 mg L^{-1} of SO_4 results in a 20-fold increase in the total Al concentration at equilibrium with Al hydroxide at pH 5 (Fig. 5A), consistent with greater concentrations of Al and SO_4 in bituminous than in anthracite discharges (Fig. 1). In contrast, neutralization and/or dilution could result in the precipitation of Al minerals.

Decreased concentration of Al and activity of Al^{3+} with increased pH are consistent with the

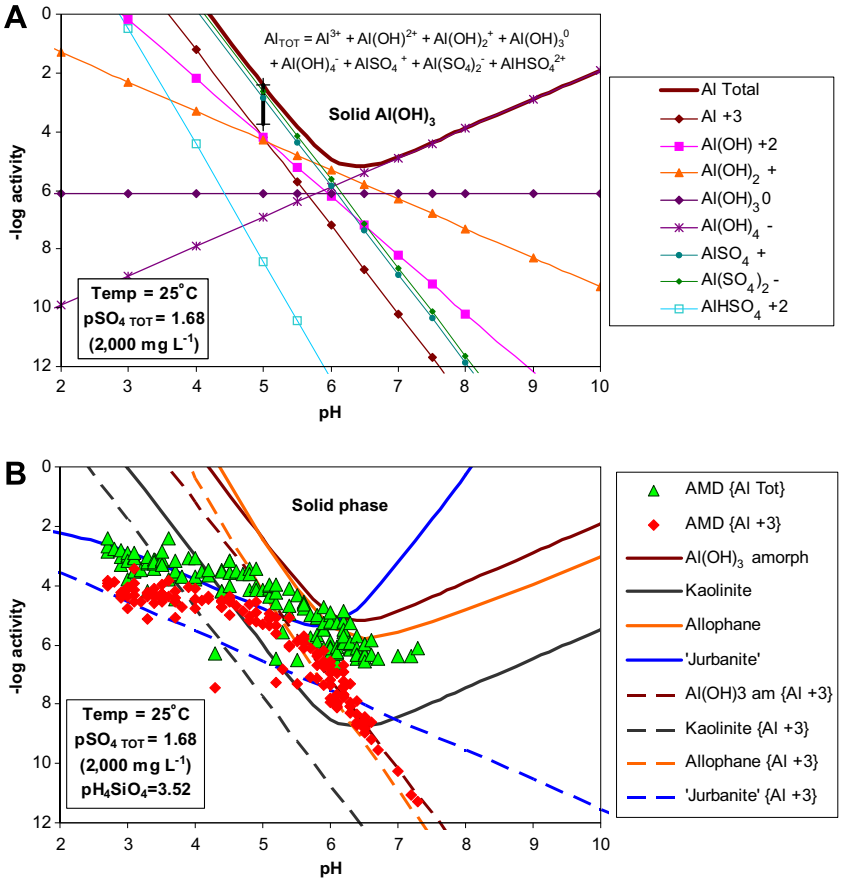

Fig. 5. Aluminum solubility at 25 °C as a function of pH and SO_4 concentration: (A) Aluminium-hydroxyl and SO_4 complexes at equilibrium with amorphous $Al(OH)_3$, 2000 mg L^{-1} total SO_4; vertical black line segment indicates solubility if SO_4 absent at pH 5. (B) Total dissolved Al and uncomplexed Al^{3+} activities for 140 CMD samples and stability limits for amorphous $Al(OH)_3$, kaolinite ($Al_2Si_2O_5(OH)_4$), "jurbanite" ($Al(SO_4)(OH) \cdot 5H_2O$), and allophane ($[Al(OH)_3]_{(1-x)}[SiO_2]_{(x)}$ where $x = 1.24–0.135 \cdot$ pH Paces (1973)). Equilibrium reactions and thermodynamic data are summarized in Table A1.

solubilities of Al hydroxide or hydroxysulfate minerals. Equilibrium computations indicated concentrations of dissolved Al and activities of Al^{3+} for the CMD samples could be limited at pH $\geqslant$ 5.5 by the precipitation of amorphous to poorly crystalline $Al(OH)_3$ and/or allophane and at pH $<$ 5.5 by an Al hydroxysulfate phase with stoichiometry and solubility similar to that for "jurbanite" (Fig. 5B). The change in slope from 1:1 at pH $<$ 5–1:3 at pH $\geqslant$ 5.5 is consistent with such solubility controls; however, Neal et al. (1987) caution about interpreting the mineral stability or stoichiometry based on the slope of Al^{3+} versus pH. The apparent saturation of CMD samples with jurbanite at low to moderate pH (Fig. 5B) is consistent with computed SI values for jurbanite ranging from −3.7 to 1.3 (Fig. 4). Amorphous Al hydroxysulfate precipitates have been reported for a variety of CMD sites (Nordstrom and Ball, 1986; Alpers et al., 1994; Robbins et al., 1996, 1999; Williams et al., 2002; Thomas and Romanek, 2002), and Al solubility control by jurbanite in CMD settings has been reported by previous researchers (Filipek et al., 1987; Cravotta, 1994; Perry, 2001). Nevertheless, Nordstrom et al. (2006) argue against solubility control of Al at pH $<$ 4.5 by jurbanite or any other mineral. Bigham and Nordstrom (2000) explained that if jurbanite or another phase with similar stoichiometry limited the concentration of dissolved Al in CMD, an inverse correlation between Al and SO_4 would be expected for low-pH samples instead of the observed positive correlation.

Speciation of Al is not sensitive to observed variations in redox potential; however, the solubilities of Fe and Mn are sensitive to redox potential in addition to pH and mineral solubilities (Bricker,

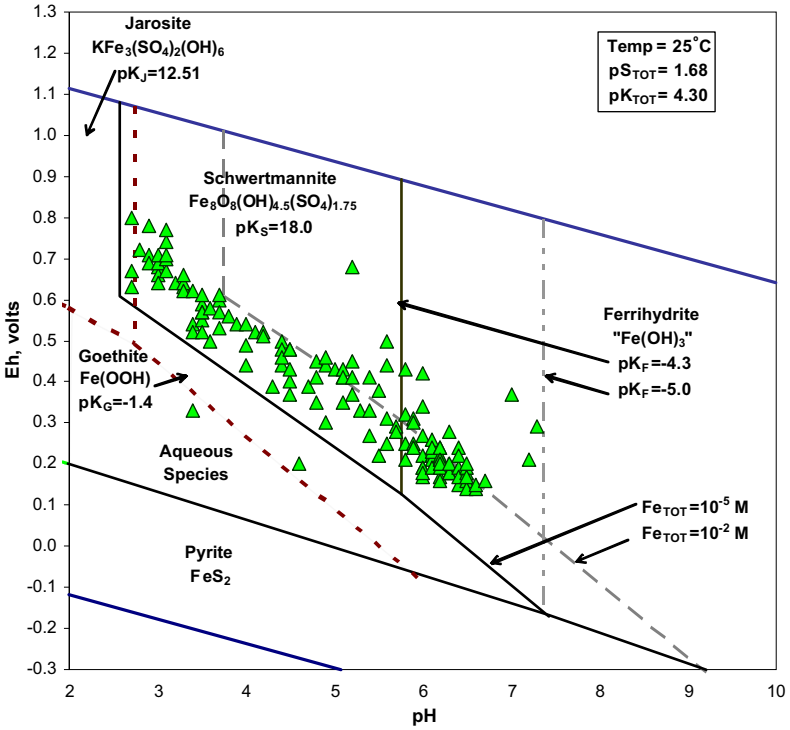

Fig. 6. Measured pH and Eh of 140 AMD samples and computed predominance areas of ferrihydrite ($Fe(OH)_3$) and schwertmannite ($Fe_8O_8(OH)_{4.5}(SO_4)_{1.75}$) relative to those of goethite (FeOOH) and jarosite ($KFe_3(SO_4)_2(OH)_6$). Thermodynamic predominance areas for aqueous species and minerals were computed assuming activities of $10^{-1.68}$ for S_{TOT} (HSO_4^-, SO_4^{-2}, H_2S, or HS^-); 10^{-4} for K_{TOT} (K^+); and 10^{-2} or 10^{-5} for Fe_{TOT} (Fe^{+2}, $FeSO_4^+$, or $FeSO_4^0$). Equilibrium reactions and thermodynamic data are summarized in Table A1.

1965; Whittemore and Langmuir, 1975; Alpers et al., 1989, 1994; Bigham et al., 1996; Yu et al., 1999, 2002; Langmuir, 1997, pp. 431–485). The measured values of pH and Eh (by Pt electrode) for this study are shown in Fig. 6 relative to the theoretical stability fields, or predominance areas, for schwertmannite ($Fe_8O_8(OH)_{4.5}(SO_4)_{1.75}$) and ferrihydrite ($Fe(OH)_3$). Mineral stability boundaries were computed for the approximate range of measured Fe concentrations, $pFe = 5$ or 2 (0.56–560 mg L^{-1}, respectively), and the maximum SO_4 concentration, $pSO_4 = 1.68$ (2000 mg L^{-1}) (Table 1). For samples in this study, the analytical concentration is approximately equal to the total activity. Most of the measured pH and Eh values plot along the stability boundaries between aqueous Fe^{II} species and Fe^{III} minerals, with a few cases plotting along mineral boundaries (Fig. 6). Although jarosite ($KFe_3(SO_4)_2(OH)_6$) and goethite (FeOOH) theoretically would be stable relative to schwertmannite and ferrihydrite (e.g. Bigham et al., 1996), the measured values for pH and Eh and the computed activities of Fe^{3+} (1) indicate "supersaturated" conditions with respect to goethite and jarosite (Fig. 7), and (2) "saturated" or near-equilibrium conditions between the aqueous species and schwertmannite or ferrihydrite. Computed saturation indices for the Fe^{III} minerals are consistent with these observations (Fig. 4). Slight supersaturation with respect to schwertmannite or ferrihydrite could indicate the presence of colloids in filtered water samples.

Ochreous precipitates were ubiquitous at the CMD sites. Nevertheless, over the range of pH (2.7–7.3) for the CMD samples, the majority of dissolved Fe was present as Fe^{II} species (Figs. 7 and 8A). Because Fe^{III} species were a minor fraction, total dissolved Fe concentrations were substantially greater than solubility limits indicated by Fe^{III} minerals (Fig. 7B). Furthermore, as with the formation of $AlSO_4$ complexes, the formation of $FeSO_4^+$ and $FeHSO_4^{2+}$ species will increase the total concentration of Fe^{III} in equilibrium with Fe^{III} hydroxide or hydroxysulfate minerals. The vertical bold line segment at pH 3 in Fig. 7A shows the addition of 2000 mg L^{-1} SO_4 and the corresponding

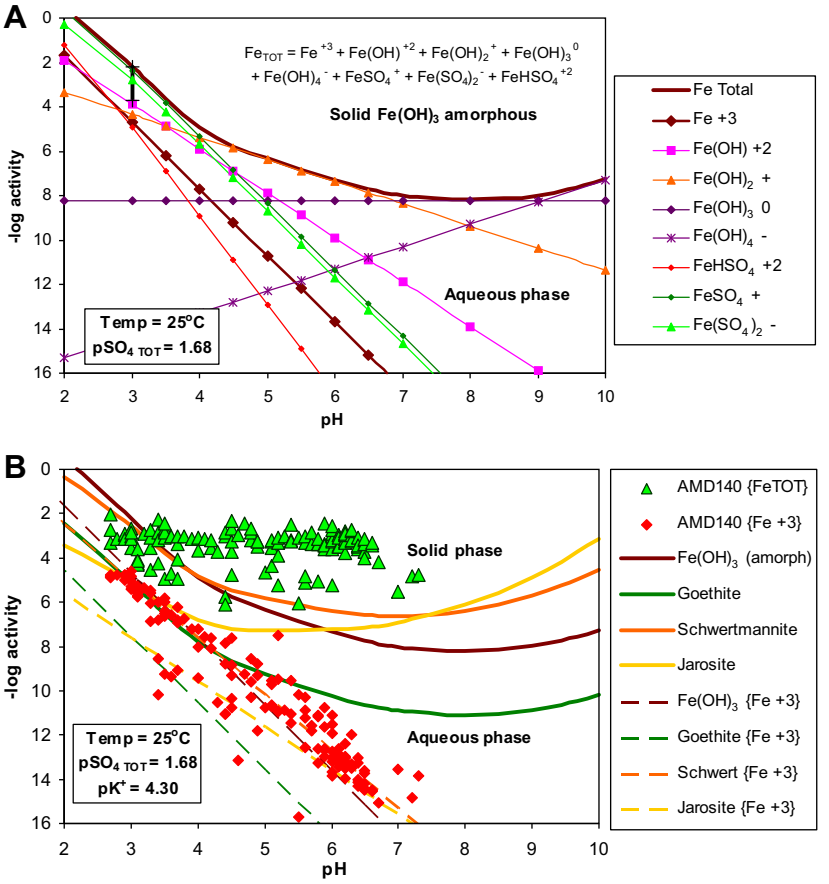

Fig. 7. Ferric iron solubility at 25 °C as a function of pH and SO_4 concentration: (A) Ferric-hydroxyl and SO_4 complexes at equilibrium with amorphous $Fe(OH)_3$, 2000 mg L^{-1} total SO_4; vertical black segment indicates solubility if SO_4 absent at pH 3. (B) Total dissolved Fe and uncomplexed Fe^{3+} activities for 140 CMD samples and potential solubility control by amorphous $Fe(OH)_3$, goethite (FeOOH), schwertmannite ($Fe_8O_8(OH)_{4.5}(SO_4)_{1.75}$), and jarosite ($KFe_3(SO_4)_2(OH)_6$). Equilibrium reactions and thermodynamic data are summarized in Table A1.

formation of Fe^{III}–SO_4 complexes can increase the total dissolved Fe concentration at equilibrium with $Fe(OH)_3$ at pH 3 by a factor of 30 (Fig. 7A), consistent with greater concentrations of Fe and SO_4 in bituminous compared to anthracite discharges at low pH (Fig. 1).

The computed activities of Fe^{3+} for the CMD samples were inversely correlated with pH and closely aligned with theoretical Fe^{3+} activity boundaries for hydrous Fe^{III} oxides and sulfates (Fig. 7B). Although variations in crystallinities and compositions of precipitated Fe^{III} phases (Whittemore and Langmuir, 1975; Yu et al., 1999) can account for some discordance between the computed Fe^{3+} activities for CMD samples and the theoretical stabilities for Fe^{III} phases at a given pH, kinetic factors also must be considered. For example, supersaturation of most CMD samples with respect to goethite can result because of kinetic barriers to the formation of this mineral and indicates goethite is unlikely to control the Fe^{3+} activities or total Fe^{III} concentrations for the CMD samples. In contrast, the apparent saturation of most CMD samples with schwertmannite and/or ferrihydrite indicates these phases are likely to precipitate and control the Fe^{3+} activities. Goethite commonly observed at CMD sites (Winland et al., 1991; Williams et al., 2002) could form by the aging and gradual transformation of metastable jarosite, schwertmannite or ferrihydrite precipitates (Miller, 1980; Bigham et al., 1996).

The poor correlation between pH and total concentrations of dissolved SO_4, Fe and Mn (Fig. 1) implies a large fraction of the metals was present as Fe^{II} and Mn^{II} (Fig. 8A and B). These reduced species were not controlled by hydroxide-mineral

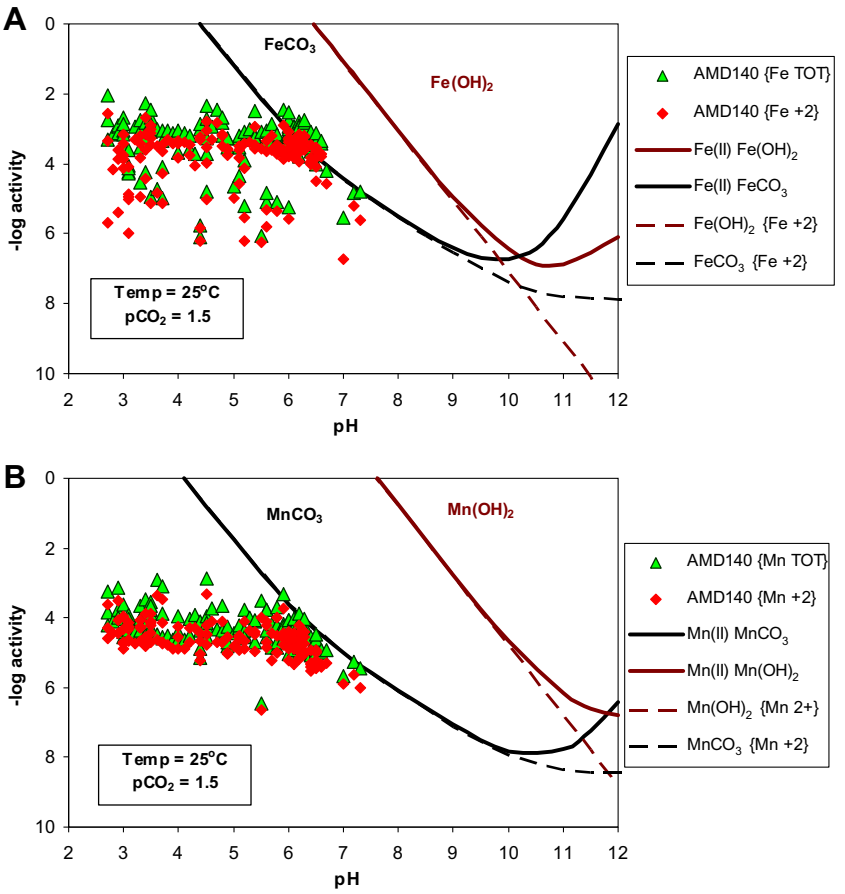

Fig. 8. Ferrous iron and Mn solubility at 25 °C as a function of pH and pCO_2: (A) Total dissolved Fe and uncomplexed Fe^{2+} activities for 140 CMD samples and potential solubility control by $Fe(OH)_2$ and siderite ($FeCO_3$). (B) Total dissolved Mn and uncomplexed Mn^{2+} activities for 140 CMD samples and potential solubility control by $Mn(OH)_2$ and rhodochrosite ($MnCO_3$). Carbonate solubility for $P_{CO_2} = 10^{-1.5}$ atm.; sulfate solubility at $SO_4 = 10^{-1.68}$ M (2000 mg L^{-1}). Equilibrium reactions and thermodynamic data are summarized in Tables A1 and A2.

solubility nor affected by SO_4 complexation under the sampled conditions ($SO_4 \leqslant 2000$ mg L^{-1} and pH $\leqslant 7.3$) to the same extent as the oxidized species.

Total concentrations of Fe and activities of Fe^{2+} were undersaturated with respect to Fe^{II} hydroxide, carbonate and sulfate minerals at low to moderate pH (pH < 6) (Fig. 8A). However, the concentrations of Fe and activities of Fe^{2+} for near-neutral pH samples approached equilibrium with siderite (Fig. 8A). Most CMD samples with pH $\geqslant$ 6 had positive SI values for siderite, ranging as high as 0.9. In contrast, all the CMD samples were undersaturated with $Fe(OH)_2$ (Fig. 8A) and melanterite; SI for melanterite was −7.4 to −2.4, indicating the Fe^{II} hydroxide and sulfate phases cannot precipitate from the CMD without increasing the pH or SO_4 concentrations, respectively.

Dissolved Mn consists entirely of Mn^{II} species for the redox conditions of the CMD samples. As with Fe^{II}, the total concentration of Mn and activity of Mn^{2+} were undersaturated with respect to Mn^{II} hydroxide, sulfate and carbonate minerals at low to moderate pH (pH < 6) (Fig. 8B). At near-neutral pH, however, the concentration of Mn could be limited by equilibrium with a carbonate phase such as rhodochrosite or impure siderite $(Fe,Mn)CO_3$ (Mozley, 1989; Morrison et al., 1990). SI values for rhodochrosite and $MnSO_4$ ranged from −4.7 to −0.1 and −13.0 to −8.8, respectively. As previously indicated, many of these samples were saturated with siderite. Large increases in pH and/or decreases in P_{CO_2} would be necessary to precipitate $Mn(OH)_2$ instead of Mn^{II}-bearing carbonates.

Although Ba and Sr concentrations increased with pH of the CMD samples (Figs. 2 and 9) and

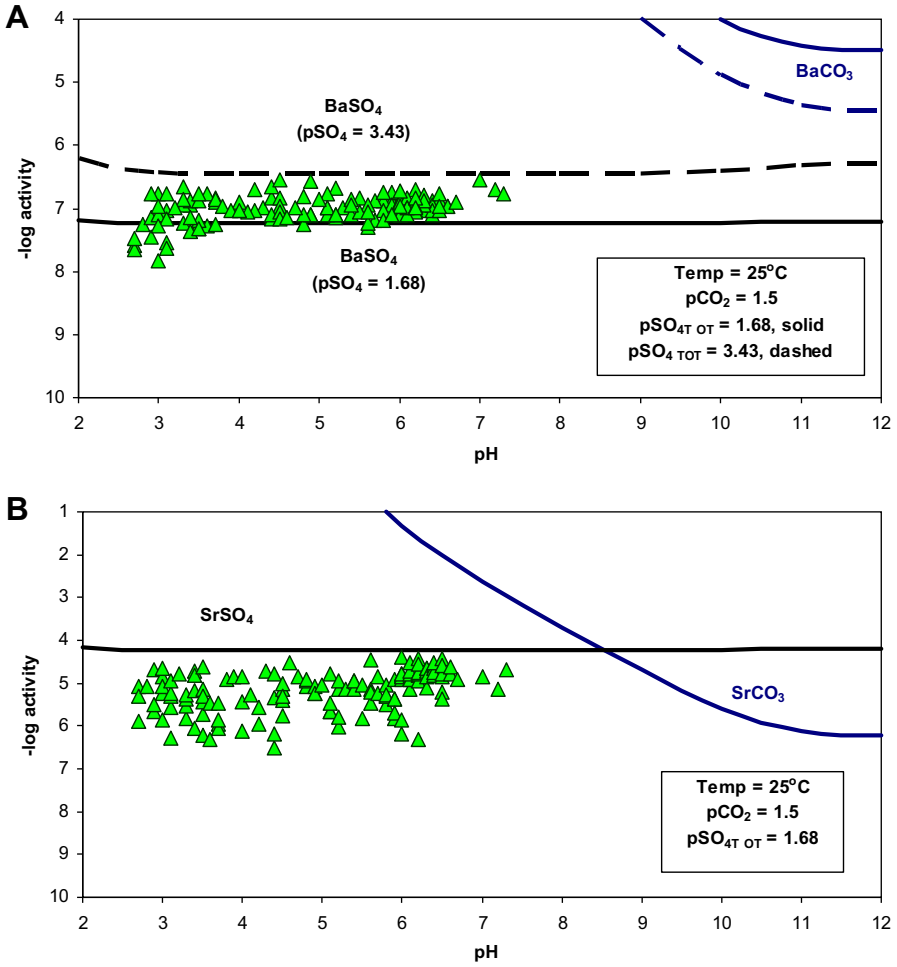

Fig. 9. Barium and Sr solubility at 25 °C as a function of pH, SO_4 and CO_3 concentrations: (A) Total dissolved Ba concentration for 140 CMD samples and potential solubility control by barite ($BaSO_4$) and witherite ($BaCO_3$). (B) Total dissolved Sr for 140 CMD samples and potential solubility control by celestite ($SrSO_4$) and strontianite ($SrCO_3$). Carbonate solubility for $P_{CO_2} = 10^{-1.5}$ atm.; sulfate solubility at $SO_4 = 10^{-1.68}$ M (2000 mg L^{-1}) or $100^{-3.43}$ M (36 mg L^{-1}). Thermodynamic data are summarized in Tables A1 and A2.

could have similar origins or fates as carbonate and sulfate minerals (Hanshaw and Back, 1979; Hanor, 1968), these two elements had different trends with respect to SO_4 concentrations in the CMD. Barium concentrations were lower in bituminous discharges than anthracite discharges for a given pH class, whereas Sr concentrations were higher in bituminous discharges than anthracite discharges (Table 1, Fig. 2). Elevated SO_4 concentrations in the bituminous discharges could have promoted the formation of insoluble barite, even at low pH (Fig. 9A). Computed SI values for barite ranged from −0.5 to 0.6 with an average value of 0.2, whereas those for witherite ranged from −9.6 to −3.7. Although Sr concentrations were greater than Ba concentrations in the CMD samples, the SI values for celestite and strontianite were less than those for the corresponding Ba minerals. The solubility boundaries for witherite and strontianite will shift downward with increased P_{CO_2}. Nevertheless, even with a pure CO_2 atmosphere ($p_{CO_2} = 10^0$ atm.), the carbonate mineral boundaries will not overlap the CMD data. Undersaturation of the CMD samples with respect to Sr minerals indicates Sr would not precipitate as a pure phase; however, Sr concentrations possibly could be controlled by its coprecipitation with barite (Hanor, 1968). Hence, the dissolution of witherite, strontianite and other carbonate minerals could be a source of dissolved Ba and Sr, whereas the precipitation and dissolution of barite could be an important control on the upper limit of Ba and Sr concentrations.

Lead and Zn concentrations decreased with increased pH but were not controlled by solubility with their respective hydroxide, carbonate or sulfate minerals (Figs. 2, 4 and 10). The CMD samples were undersaturated with respect to various sulfate, carbonate, or hydroxide phases included in WATEQ4F (Ball and Nordstrom, 1991). Concentrations of Pb generally were greater in anthracite discharges than bituminous discharges. Highest Pb concentrations, from 7 to 11 μg L^{-1}, were found in several anthracite discharges over a range of pH values (Table 1, Fig. 2). In contrast, Zn concentrations generally were comparable between anthracite and bituminous discharges with similar pH and were 10–100 times larger than those of Pb, ranging from <1 to 10,000 μg L^{-1}. Declines in Pb and Zn concentrations with increased pH did not result from solubility control by carbonate minerals, such as cerrusite or smithsonite. Although smaller concentrations of Pb in bituminous discharges with elevated SO_4 concentrations are consistent with solubility control by a sulfate phase, such as anglesite, concentrations of Pb were highly undersaturated with respect to anglesite. Possibly, Pb could be precipitated as an impurity with barite. Hammarstrom et al. (2006) reported finding barite in sedimentary rock samples associated with coal deposits; however, data are not available on the composition of barite at the CMD sites. Hence, concentrations of dissolved Pb and Zn in the CMD samples must be limited by mechanisms

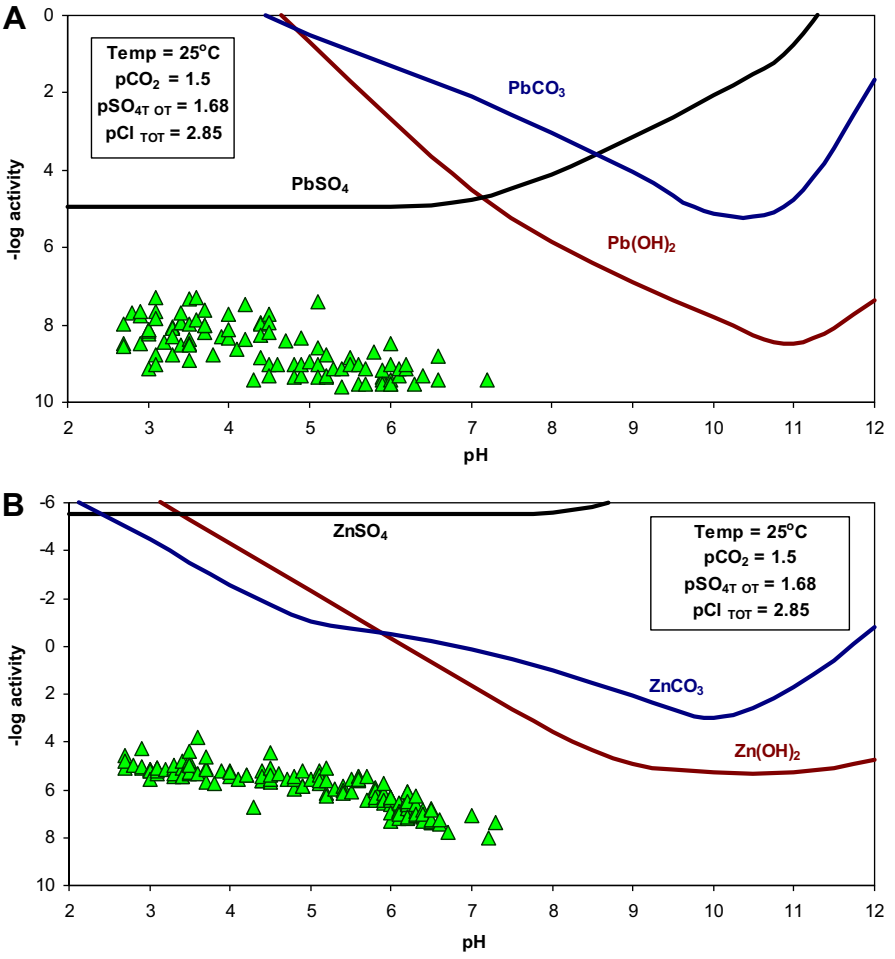

Fig. 10. Lead and Zn solubility at 25 °C as a function of pH, SO_4, Cl and CO_3 concentrations: (A) Total dissolved Pb concentration for 140 CMD samples and potential solubility control by anglesite ($PbSO_4$) and cerrusite ($PbCO_3$). (B) Total dissolved Zn for 140 CMD samples and potential solubility control by $Zn(OH)_2$, smithsonite ($ZnCO_3$), and zincosite ($ZnSO_4$). Carbonate solubility for "open system" ($P_{CO_2} = 10^{-1.5}$); sulfate solubility for $SO_4 = 10^{-1.68}$ M (2000 mg L^{-1}). Equilibrium reactions and thermodynamic data are summarized in Tables A1, A2 and A3.

such as coprecipitation with barite or another SO_4-bearing phase and/or adsorption on hydrous Fe^{III} oxides as explained below.

Elevated concentrations of Ba and Pb in "dilute," greater volume anthracite discharges compared to "mineralized" bituminous discharges are noteworthy considering interests for developing water resources and extracting metals at abandoned mine sites. Although the anthracite water resource may contain acceptable concentrations of SO_4 for industrial and domestic uses, the concentrations and mass loadings of Ba and Pb warrant consideration relative to the end use. Increasing concentrations of SO_4 in solution may be beneficial for decreasing concentrations of Ba, Pb, and other potentially toxic constituents. Sulfate could facilitate the removal of elements such as Ba and Pb as sulfate compounds at relatively low pH, whereas major ions such as Ca, Mg, Mn^{II}, and Fe^{II} ions remain in solution. At least one commercial process that may be used to treat CMD to meet water-quality standards involves the removal of SO_4 by the introduction of $BaCl_2$ and the subsequent reductive dissolution of the $BaSO_4$ precipitate (Maree et al., 2004).

Cu and Cd concentrations decreased sharply with increased pH, with Cu concentrations consistently a factor of 10 or greater than those of Cd (Figs. 2 and 11). Neither Cu nor Cd approached saturation with their respective sulfate, hydroxide or carbonate solids (Fig. 11) included in WATEQ4F (Ball and Nordstrom, 1991), indicating solubility

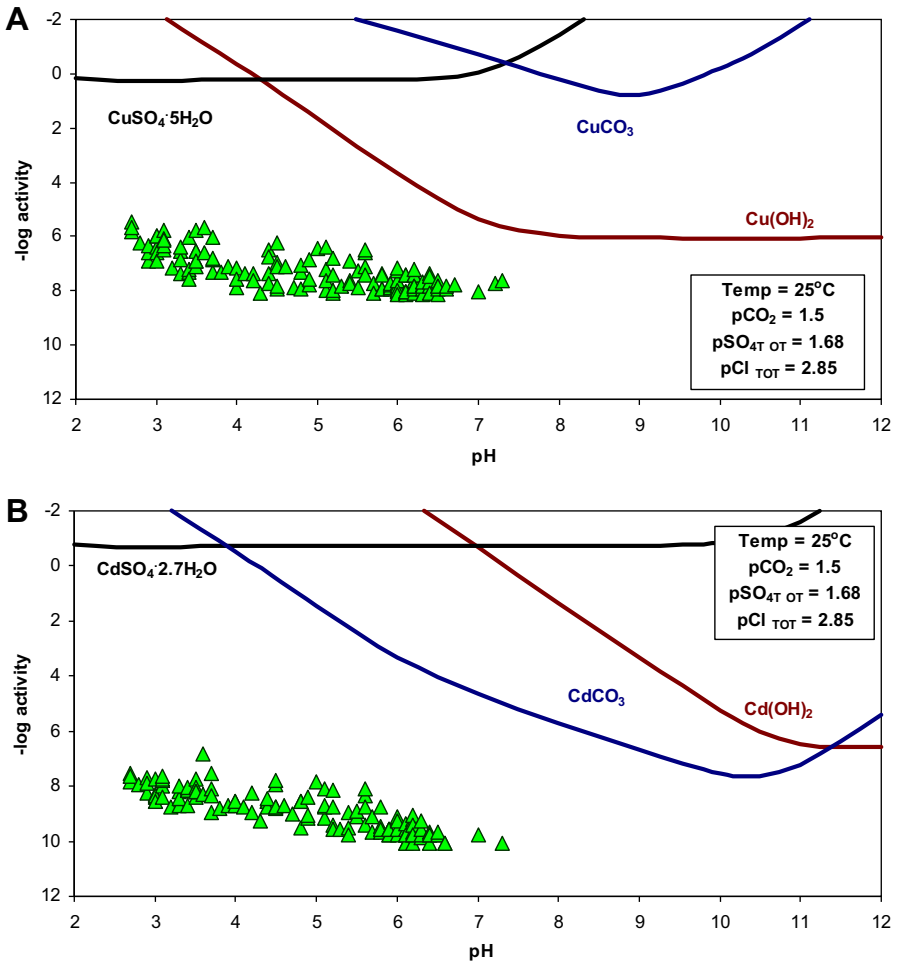

Fig. 11. Copper and Cd solubility at 25 °C as a function of pH, SO_4, Cl and CO_3 concentrations: (A) Total dissolved Cu for 140 CMD samples and potential solubility control by $Cu(OH)_2$, $CuCO_3$ and chalcanthite ($CuSO_4$). (B) Total dissolved Cd for 140 CMD samples and potential solubility control by $Cd(OH)_2$, otavite ($CdCO_3$), and cadmium sulfate ($CdSO_4 \cdot 2.7H_2O$). Carbonate solubility for $P_{CO_2} = 10^{-1.5}$ atm.; sulfate solubility for $SO_4 = 10^{-1.68}$ M (2000 mg L^{-1}). Thermodynamic data are summarized in Tables A1 and A2.

control by secondary minerals is unlikely. It is unlikely that Cu concentrations are limited by the lack of supply, because coal and associated black shales are enriched sources of Cu (Mason, 1966; Bragg et al., 1997). Hence, observed concentrations of dissolved Cu and Cd in the CMD samples could be controlled by adsorption.

4.2. Surface complexation controls of constituents in CMD samples

Surface-complexation, or adsorption–desorption reactions between cations and anions and Fe^{III} hydroxides or hydroxysulfates could account for the undersaturation of Pb, Zn, Ni, Cu and Cd with respect to various hydroxide, carbonate, or sulfate minerals; inverse correlations between pH and concentrations of Pb, Zn, Ni, Cu and Cd; the positive correlations between pH and concentrations of As and, to a lesser extent, B; and the lack of correlation between pH and Se concentrations (Fig. 2). Simulated effects of adsorption and desorption of dissolved cation and anion concentrations on suspended particles of "HFO" are illustrated as a function of pH in Fig. 12. These illustrations show the equilibrium percentages of the total constituent concentration in solution and that adsorbed at a given pH and can be compared with prior illustrations showing dissolved constituent concentrations as a function of pH (Figs. 1–11). However, because of the wide ranges in metal concentrations and unknown quantities, chemical characteristics, and physical properties of sorbent at the CMD sites, only qualitative comparisons between the simulated and observed concentration trends can be considered.

Simulated distributions for the sorption of cations on HFO as a function of pH (Fig. 12A) generally mimic the observed trends between these constituents and pH, with decreased dissolved concentrations in the order of lowest pH of sorption: $Pb < Cu < Zn < Cd < Ba = Mn < Sr < Ni$. The simulated sorption equilibria indicate that Ba, Mn, Sr and Ni would not be strongly controlled by adsorption over the pH range of 2.7–7.3 for the CMD samples. Only 5% or less of the initial concentrations of these cations are indicated as adsorbed at $pH \leqslant 7.3$, whereas 95% or more remains dissolved. In contrast, 20% or more of the initial concentrations of Cd, Zn, Cu or Pb could be adsorbed at pH 7.3. The concentrations of Pb, Zn, Cu and Cd in the CMD samples begin to show a significant inverse correlation with pH between pH 3.5 and pH 5.5 (Figs. 10 and 11), consistent with the sorption model results (Fig. 12A). Hence, Pb, Zn, Cu and Cd concentrations in the CMD samples could be limited by adsorption on HFO and associated solids. The widespread occurrence of ochres at the CMD sites and the tendency for adsorption of Pb, Zn, Cu, and Cd at slightly acidic pH helps to explain their persistent undersaturation with respect to their corresponding sulfate, carbonate or hydroxide phases.

Simulated distributions for the sorption of As (arsenate plus arsenite), Se (selenite plus selenate), B (borate), and S (sulfate) on HFO as a function of pH (Fig. 12B) also mimic trends between these constituents and pH, with decreased dissolved concentrations in the order of lowest pH of sorption: $As < Se < SO_4 < BO_3$. Generally, concentrations of SO_4 and BO_3 are minimally affected by sorption on HFO. In contrast, at pH 7.3, more than 50% of the initial concentrations of As and Se may be adsorbed by HFO.

At the pH and Eh of the CMD samples, H_3AsO_4 and $H_2AsO_4^-$ species would predominate (e.g. Bowell, 1994; Smedley and Kinniburgh, 2002). Arsenic concentrations are greatest at pH less than 3, are least at pH 3–4, and then increase with increased pH (Fig. 2). Furthermore, As concentrations are weakly correlated with SO_4 and are greater in bituminous CMD than in anthracite CMD. These trends are consistent with adsorption–desorption control by HFO (Fig. 12) and the potential for competitive desorption of As when concentrations of SO_4 become elevated. For CMD with pH less than 2.3, the HFO sorbents tend to be soluble (Figs. 6 and 7); hence, observed As concentrations tend to be elevated in the lowest pH samples. However, with increased pH, HFO can precipitate; H_3AsO_4 and $H_2AsO_4^-$ ions can adsorb (Fig. 12). At pH 3–4, more than 90% of the As may be adsorbed. However, with increased pH desorption results, and the dissolved concentration of As increases at the expense of the adsorbed fraction. Sulfate can compete with and displace As from sorption sites. Nevertheless, As adsorption is stronger than SO_4 in sorption models (Fig. 12), and the As/S ratio in coal is 1000 times that of mine drainage (Cravotta et al., 2001). This indicates that As is strongly attenuated in the aqueous environment compared to SO_4. Dilution would not affect the As/S ratio; hence, the attenuation must result from adsorption or other mechanisms that can decrease the concentration of As but not SO_4.

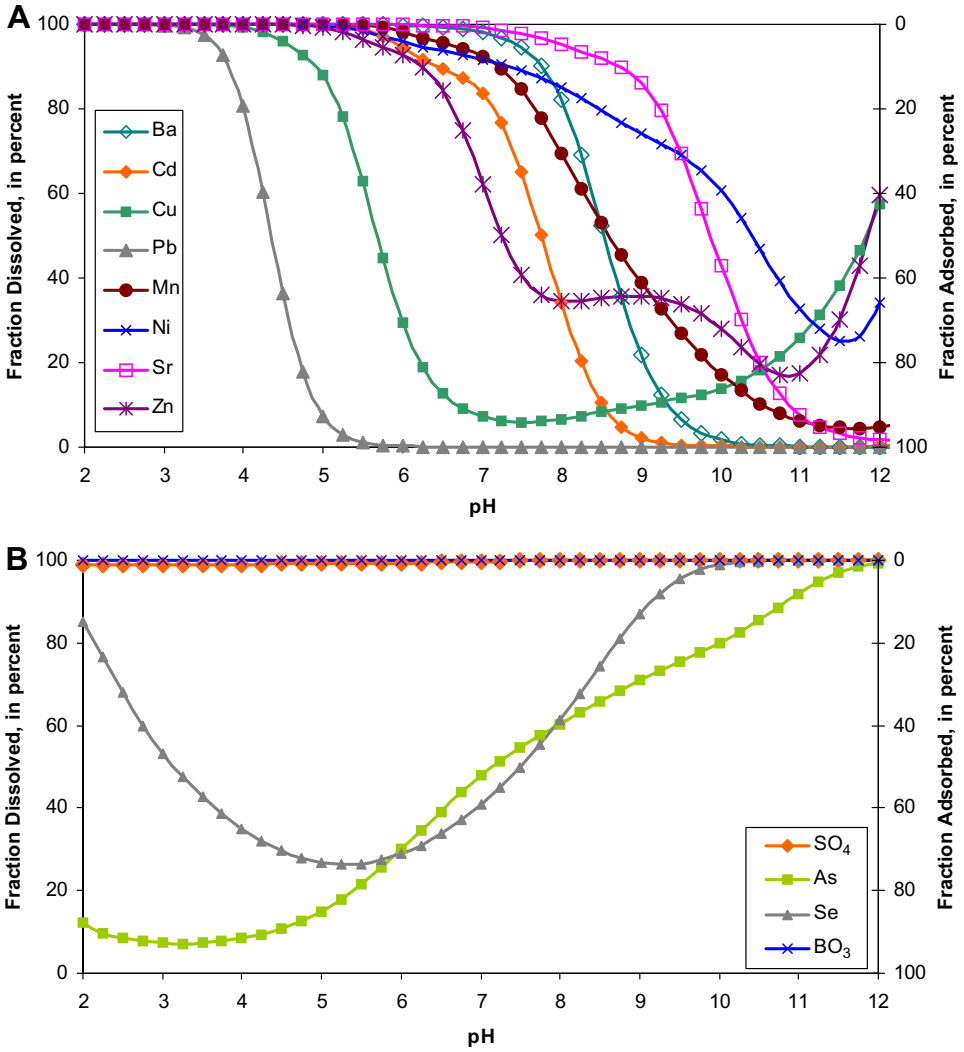

Fig. 12. Equilibrium fractions of initial concentrations of cations and anions that are dissolved or adsorbed on a finite amount of hydrous ferric oxide at 25 °C as a function of pH: (A) Cations – Ba, Cd, Cu, Pb, Mn, Ni, Sr, and Zn. (B) Anions – As (arsenite plus arsenate), borate, Se (selenite plus selenate), and SO_4. Area below curve indicates fraction that is not adsorbed; area above curve indicates fraction adsorbed. Simulations conducted using PHREEQC (Parkhurst and Appelo, 1999) with thermodynamic data from Ball and Nordstrom (1991) and surface-complexation data from Dzombak and Morel (1990).

Unlike As, Se concentrations were not correlated with pH. Highest Se concentrations, from 5 to 7.6 μg L^{-1}, were found in several bituminous discharges with a range of pH values. The poor correlation between Se concentrations and pH results because the sorption trends are not linear over the range of pH of CMD samples. The simulated distribution for the sorption of Se (selenate plus selenite) indicates increased adsorption with increased pH to 5, followed by desorption with continued increases in pH. The observed medians for specific pH classes are smaller at pH 4–5 than at lower or higher pH values (Fig. 2), consistent with strong adsorption control of Se at intermediate pH.

4.3. Mixing of CMD with oilfield brine

The surface-complexation of As by HFO (Fig. 12) is consistent with the observed trends for As and pH, but requires oxidizing conditions. Nevertheless, many of the CMD samples were suboxic to anoxic (Table 1). The mobilization of As at near-neutral pH could result by the reductive dissolution of Fe^{III} oxides and the consequent release of

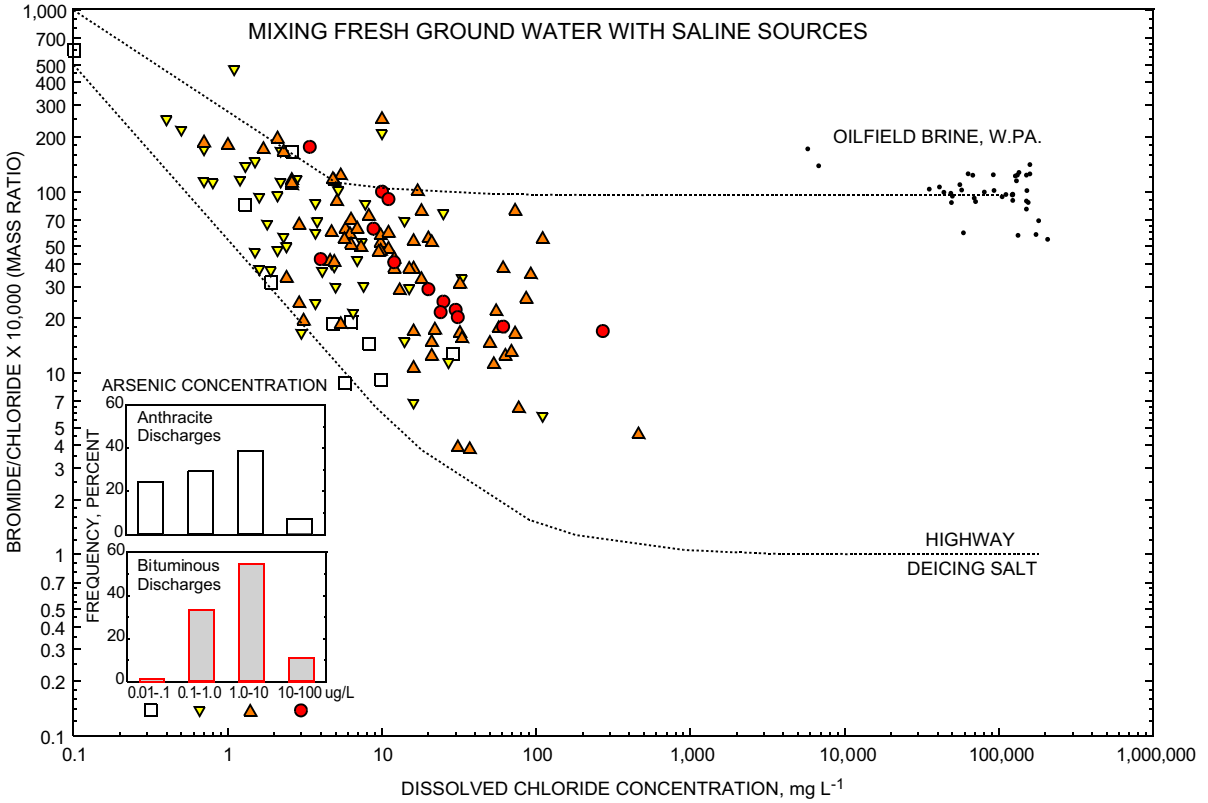

Fig. 13. Bromide/Cl ratios and Cl concentrations for 140 abandoned mine discharge samples, Pennsylvania, 1999 (this study), and oilfield brines from Western Pennsylvania (Dresel, 1985), with symbols for data from this study to indicate possible As contributions from interaction with saline sources (adapted from Whittemore, 1988).

any adsorbed or coprecipitated constituents (Bowell, 1994; Smedley and Kinniburgh, 2002). Although the two highest concentrations of As were in low-pH and high-Eh discharges (Fig. 2), positive correlations between As and pH, Na, Cl, I and Br and an inverse correlation between As and Eh were apparent for the 140 CMD samples (Cravotta, 2008). Such correlations indicate the possible mobilization of As by reductive dissolution of Fe^{III} oxides and/or competitive adsorption of Cl. Anaerobic, saline conditions may be present within certain underground mines. Saline ground water associated with oilfield brines has been documented in western Pennsylvania (Dresel, 1985), and discharges of CMD and brines from abandoned oil and gas exploration holes is a serious problem in some localities (Hedin et al., 2005). The maximum concentrations of Cl and Na for the 140 CMD samples were 460 and 500 mg L^{-1}, respectively (Cravotta, 2008, Table 2).

Whittemore (1988) demonstrated that the concentration of Br in halite used as road deicing salts is less than that in oilfield brines, and that ground water that is a mixture of freshwater and either of these two salt sources may be distinguished on the basis of the Br/Cl ratio. The Br/Cl ratio for a mixture of freshwater with road salt approaches 0.0001 with increased contributions from the salt source, whereas that in oilfield brine approaches 0.01 (Fig. 13). Using different symbols to indicate different concentrations of As in CMD samples, a plot of Br/Cl and Cl indicates the highest concentrations of As were observed for samples that have elevated Cl but intermediate compositions between the two end-member salt sources. Hence, deep ground water may be a mixture of various sources, consistent with the general trend of increased As and Cl concentrations.

5. Summary and conclusions

Regional water-quality data were collected in 1999 for 140 abandoned underground mines in Pennsylvania. The pH ranged from 2.7 to 7.3, with

the majority of samples having pH 2.5–4.0 (acidic) or pH 6.0–7.0 (near neutral). Generally bituminous discharges had smaller flow rates and were more mineralized than anthracite discharges with similar pH; flow rate increased with pH of the discharges. Increased pH with increased flow rate is consistent with dilution of initially acidic CMD with alkaline water or with less extensive reactions because of decreased mineral-water contact with high flows. Dilution effects were more pronounced for anthracite discharges than bituminous discharges.

Bituminous discharges had higher median and maximum concentrations of alkalinity, acidity, SO_4, Fe, Al, Mn, As, B, Cu, Ni, Se and Zn than anthracite discharges, but lower median concentrations of dissolved Ba and Pb. Positive correlations between SO_4 and other constituents indicate similar origin, similar solubility-control mechanisms, and/or potential for ion-pairing.

Formation of $AlSO_4^+$ and $AlHSO_4^{2+}$ complexes adds to the total dissolved Al concentration at equilibrium with Al hydroxide or hydroxysulfate minerals and can account for 10–20 times greater concentrations of dissolved Al in bituminous discharges compared to anthracite discharges at similar pH. Similarly, the formation of $FeSO_4^+$ and $FeHSO_4^{2+}$ increases the solubility of Fe^{III} in equilibrium with Fe^{III} hydroxide or hydroxysulfate minerals.

Dissolved Al, Zn, and Pb concentrations were inversely correlated with pH, whereas SO_4, Fe, Mn and Ba concentrations were not correlated or weakly correlated with pH. Inverse correlations between the pH and concentrations of Al and other metals could be a result of solubility control by hydroxide, hydroxysulfate, and/or carbonate minerals. Concentrations of Al and activities of Al^{3+} at pH $\geqslant$ 3.5 for the CMD samples were at equilibrium with amorphous to poorly crystalline $Al(OH)_3$, allophane, and/or kaolinite. Similarly, the activities of Fe^{3+} at pH $\geqslant$ 3.5 were controlled by equilibrium with $Fe(OH)_3$ or schwertmannite. Nevertheless, dissolved Fe and Mn in most samples were dominated by relatively soluble Fe^{II} and Mn^{II} species. At pH $>$ 6, the precipitation of siderite, rhodochrosite, or mangano-siderite could limit the maximum concentration of dissolved Fe and Mn.

High solubilities for various carbonate minerals compared to dissolved Ca, Fe, Mn, Ba, Pb and Zn, particularly at pH $<$ 6, indicate the carbonate minerals could be important sources of dissolved constituents in the mine drainage samples. However, additional qualitative and quantitative information on the composition and solubilities of impure carbonate minerals would be needed to determine the actual sources and sinks of these elements.

Higher SO_4 concentrations but lower Pb and Ba concentrations in bituminous than anthracite discharges indicate increased SO_4 concentration has a negative effect on the solubility of these metals. Modeling results suggest that most samples were saturated with barite, but none were saturated with anglesite. Lead potentially could be precipitated as an impurity with barite and/or controlled by adsorption to schwertmannite or another Fe^{III} hydroxide. Concentrations of other trace elements, including Cu, Cd, Ni, Zn, Se, and As, also may be controlled by adsorption processes.

Although the two highest concentrations of As were in low-pH and high-Eh discharges, generally the concentration of As increased with increased pH and decreased Eh. Concentrations of As were positively correlated with Cl and other halides, Fe and SO_4 (in order of decreased significance). These relationships imply that dissolved As in mine discharges generally results from (1) weathering of pyrite and other minerals associated with coal deposits under oxidizing conditions, and (2) reductive dissolution of oxides along flow paths of deep, reducing ground waters. Attenuation of As in mine discharges results from (1) adsorption to ochre-forming "$Fe(OH)_3$" that precipitates under oxidizing conditions, and (2) to a lesser degree, dilution. The same mechanisms apply to other mineral constituents particularly those that are affected by the oxidation of sulfides or adsorption.

In conclusion, thermodynamic equilibrium models that consider mineral solubility, aqueous speciation, and surface-complexation reactions can be useful to explain complex relations among the pH, SO_4 and dissolved metals for mine discharges. The application of such models provides a basis for determining the significance of various geochemical processes that control water quality. In CMD, concentrations of Fe^{III} and Al tend to be limited by hydroxide-mineral solubilities, whereas concentrations of Fe^{II} and Mn^{II} tend to be limited by carbonate-mineral solubilities. Concentrations of Ba and, to a lesser extent, Sr and Ca tend to be limited by sulfate-mineral solubilities at low pH and carbonate solubilities at neutral to alkaline pH. In contrast, Cd, Cu, Pb and Zn concentrations tend to be substantially less than equilibrium with respect to

solubility limits for hydroxide, carbonate, or sulfate minerals. Concentrations of these trace metals and oxyanions, such as As, Se, and B, in CMD tend to be limited to low values by surface-complexation reactions with Fe^{III} minerals such as schwertmannite, ferrihydrite, and goethite. Although the occurrence of such ochre-forming minerals at CMD sites generally is considered an environmental liability, the formation of fresh Fe^{III} minerals helps to attenuate the transport of toxic elements such as As, Cd, Cu, Pb and Zn. Ochres that have potential for economic utilization as Fe^{III}-oxide pigments or other applications may need to be relatively free of impurities (e.g. Hedin, 2003). Thus, an understanding of the processes that control trace-element concentrations in CMD or associated solids can be helpful in the design of treatment systems that can reduce contaminant transport, yield ochres free of specific impurities, or capture potentially valuable constituents from the CMD.

Acknowledgments

This work was conducted by the U.S. Geological Survey (USGS), in cooperation with the Southern Alleghenies Conservancy (SAC), and with support from the U.S. Environmental Protection Agency (USEPA) and the Pennsylvania Department of Environmental Protection (PaDEP). The author wishes to thank his USGS colleagues, Donald R. Williams (retired) and Jeffrey B. Weitzel for field and laboratory assistance and Nadine Piatak and Jane Hammarstrom for analytical support. Bernie Sarnoski, Brandon Diehl, and Brad Clemenson provided both encouragement and support. The manuscript benefitted from reviews by Kevin J. Breen, Robert R. Seal II, Briant Kimball and Arthur W. Rose.

Appendix A. Supplementary material

Supplementary data associated with this article can be found, in the online version, at doi:10.1016/j.apgeochem.2007.10.003.

References

Alpers, C.N., Nordstrom, D.K., Ball, J.W., 1989. Solubility of jarosite solid solutions precipitated from acid mine waters, Iron Mountain, California, U.S.A. Sci. Geol. Bull., Strasbourg 42, 281–298.

Alpers, C.N., Blowes, D.W., Nordstrom, D.K., Jambor, J.L., 1994. Secondary minerals and acid mine water chemistry. In: Jambor, J.L., Blowes, D.W. (Eds.), Environmental Geochemistry of Sulfide Mine-Wastes. Mineralogical Association of Canada, Short Course Handbook, vol. 22, pp. 247–270.

American Public Health Association, 1998. Alkalinity (2320)/titration method. In: Clesceri, L.S., Greenberg, A.E., Eaton, A.D. (Eds.), Standard Methods for the Examination of Water and Wastewater, 20th ed. American Public Health Association, Washington, DC, pp. 2.26–2.29.

Baker, J.P., Schofield, C.L., 1982. Aluminum toxicity to fish in acidic waters. Water Air Soil Pollut. 18, 289–309.

Ball, J.W., Nordstrom, D.K., 1991. User's manual for WATEQ4F with revised data base. U.S. Geological Survey. Open-File Rep. 91-183, 189 p. <http://wwwbrr.cr.usgs.gov/projects/GWC_chemtherm/pubs/wq4fdoc.pdf> (accessed on the Word Wide Web on July 13, 2004).

Barnes, I., Clarke, F.E., 1969. Chemical properties of ground water and their corrosion and encrustation effects on wells. U.S. Geological Survey. Prof. Paper 498-D, pp. D1–D58.

Berg, T.M., Barnes, J.H., Severn, W.D., Skema, V.K., Wilshusen, J.P., Yannaci, D.S., 1989. Physiographic provinces of Pennsylvania. Pennsylvania Geological Survey, fourth series, Map 13, scale 1:2,000,000.

Bigham, J.M., Nordstrom, D.K., 2000. Iron and aluminum hydroxysulfate minerals from acid sulfate waters. In: Jambor, J.L., Alpers, C.N., Nordstrom, D.K. (Eds.), Sulfate Minerals, Crystallography, Geochemistry and Environmental Significance, vol. 40. Mineralogical Society of America Reviews in Mineralogy and Geochemistry, pp. 351–403.

Bigham, J.M., Schwertmann, U., Traina, S.J., Winland, R.L., Wolf, M., 1996. Schwertmannite and the chemical modeling of iron in acid sulfate waters. Geochim. Cosmochim. Acta 60, 2111–2121.

Blowes, D.W., Ptacek, C.J., 1994. Acid-neutralization mechanisms in inactive mine tailings. In: Jambor, J.L., Blowes, D.W. (Eds.), Environmental Geochemistry of Sulfide Mine-Wastes. Mineralogical Association of Canada, Short Course Handbook, vol. 22, pp. 271–292.

Bowell, R.J., 1994. Sorption of arsenic by iron oxides and oxyhydroxides in soils. Appl. Geochem. 9, 279–286.

Bragg, L.J., Oman, J.K., Tewalt, S.J., Oman, C.J., Rega, N.H., Washington, P.M., Finkelman, R.B., 1997. U.S. Geological Survey Coal Quality (COALQUAL) Database, Version 2.0. U.S. Geological Survey. Open-File Rep. 97-134.

Bricker, O.P., 1965. Some stability relations in the system Mn–O_2–H_2O at 25 × C and one atmosphere total pressure. Am. Mineral 50, 1296–1354.

Coston, J.A., Fuller, C.C., Davis, J.A., 1995. Pb^{2+} and Zn^{2+} adsorption by a natural aluminum- and iron-bearing surface coating on an aquifer sand. Geochim. Cosmochim. Acta 59, 3535–3547.

Cravotta III, C.A., 1994. Secondary iron-sulfate minerals as sources of sulfate and acidity – the geochemical evolution of acidic ground water at a reclaimed surface coal mine in Pennsylvania. In, Alpers, C.N., Blowes, D.W. (Eds.), Environmental Geochemistry of Sulfide Oxidation. American Chemical Society of Symposium Series, vol. 550, pp. 345–364.

Cravotta III, C.A., 2005. Effects of abandoned coal-mine drainage on streamflow and water quality in the Mahanoy Creek Basin, Schuylkill, Columbia, and Northumberland Counties, Pennsylvania, 2001. U.S. Geological Survey. Scientific Invest. Rep. 2004-5291.

Cravotta III, C.A., 2008. Dissolved metals and associated constituents in abandoned coal-mine discharges, Pennsylvania,

USA. Part 1: Constituent quantities and correlations. Appl. Geochem. 23, 166–202.

Cravotta III, C.A., Bilger, M.D., 2001. Water-quality trends for a stream draining the Southern Anthracite Field, Pennsylvania. Geochem. Explor. Environ. Anal. 1, 33–50.

Cravotta III, C.A., Trahan, M.K., 1999. Limestone drains to increase pH and remove dissolved metals from acidic mine drainage. Appl. Geochem. 14, 581–606.

Cravotta III, C.A., Dugas, D.L., Brady, K.B.C., Kovalchuk, T.E., 1994. Effects of selective handling of pyritic, acid-forming materials on the chemistry of pore gas and ground water at a reclaimed surface coal mine in Clarion County, PA, USA. U.S. Bureau of Mines Spec. Publ. SP 06A, pp. 365–374.

Cravotta III, C.A., Brady, K.B.C., Rose, A.W., Douds, J.B., 1999. Frequency distribution of the pH of coal-mine drainage in Pennsylvania. In: Morganwalp, D.W., Buxton, H. (Eds.), U.S. Geological Survey Toxic Substances Hydrology Program – Proceedings of the Technical Meeting. U.S. Geological Survey. Water Resource Invest. Rep. 99-4018A, pp. 313–324.

Cravotta III, C.A., Breen, K.J., Seal II, R.R., 2001. Arsenic is ubiquitous but not elevated in abandoned coal-mine discharges in Pennsylvania (abs.). In: U.S. Geological Survey Appalachian Region Integrated Science Workshop Proceedings, Gatlinburg, Tennessee, October 22–26, 2001. U.S. Geological Survey. Open-File Rep. 01-406, p. 105.

Crock, J.G., Arbogast, B.F., Lamothe, P.J., 1999. Laboratory methods for the analysis of environmental samples. In: Plumlee, G.S., Logsdon, M.J. (Eds.), The Environmental Geochemistry of Mineral Deposits – Part A. Processes, Techniques, and Health Issues. Society of Economic Geologists, Reviews in Economic Geology 6A, 265–287.

Davis, J.A., Kent, D.B., 1990. Surface complexation modeling in aqueous geochemistry. In: Hochella, M.F., Jr., White, A.F. (Eds.), Mineral–Water Interface Geochemistry, vol. 23. Mineralogical Society of America Reviews in Mineralogy and Geochemistry, pp. 177–260.

Dresel, P.E., 1985. The geochemistry of oilfield brines from western Pennsylvania. University Park, Pennsylvania State University, M.S. thesis.

Drever, J.I., 1997. The Geochemistry of Natural Waters-Surface and Groundwater Environments, third ed. Prentice-Hall Inc., Englewood Cliffs, NJ.

Dzombak, D.A., Morel, F.M.M., 1990. Surface Complexation Modeling-Hydrous Ferric Oxide. John Wiley & Sons Inc., New York.

Earle, J., Callaghan, T., 1998. Effects of mine drainage on aquatic life, water uses, and man-made structures. In: Brady, K.B.C., Smith, M.W., Schueck, J.H. (Eds.), Coal Mine Drainage Prediction and Pollution Prevention in Pennsylvania. Harrisburg, Pennsylvania Department of Environmental Protection, 5600-BK-DEP2256, pp. 4.1–4.10.

Edmunds, W.E., 1999. Bituminous coal. In: Schultz, C.H. (Ed.), The Geology of Pennsylvania. Pennsylvania Geological Survey, fourth series, Spec. Publ. 1, pp. 470–481.

Eggleston, J.R., Kehn, T.M., Wood Jr., G.H., 1999. Anthracite. In: Schultz, C.H. (Ed.), The Geology of Pennsylvania. Pennsylvania Geological Survey, 4th series, Spec. Publ. 1, pp. 458–469.

Elder, J.F., 1988. Metal biogeochemistry in surface-water systems–a review of principles and concepts. U.S. Geological Survey Circular 1013.

Ficklin, W.H., Mosier, E.L., 1999. Field methods for sampling and analysis of environmental samples for unstable and selected stable constituents. In: Plumlee, G.S., Logsdon, M.J. (Eds.), The Environmental Geochemistry of Mineral Deposits – Part A. Processes, Techniques, and Health Issues. Society of Economic Geologists, Reviews in Economic Geology 6A, 249–264.

Filipek, L.H., Nordstrom, D.K., Ficklin, W.H., 1987. Interaction of acid mine drainage with waters and sediments of West Shaw Creek in the West Shasta Mining District, California. Environ. Sci. Technol. 21, 388–396.

Fishman, M.J., Friedman, L.C. (Eds.), 1989. Methods for Determination of Inorganic Substances in Water and Fluvial Sediments. U.S. Geological Survey. Tech. Water Resource Invest., Book 5, Chapter A1.

Foster, M.D., 1950. The origin of high sodium bicarbonate waters in the Atlantic and Gulf Coastal Plains. Geochim. Cosmochim. Acta 1, 33–48.

Hammarstrom, J.M., Smith, K.S., 2002. Geochemical and mineralogic characterization of solids and their effects on waters in metal-mining environments. In: Seal II, R.R., Foley, N.K. (Eds.), Progress on Geoenvironmental Models for Selected Mineral Deposit Types. U.S. Geological Survey. Open-File Rep. 02-195, pp. 9–54.

Hammarstrom, J.M., Cravotta, C.A., Brady, K., Hornberger, R., Jackson, J., Dulong, F., Galeone, D., 2006. Geochemical and mineralogical characterization of overburden materials for the ADTI-WP2 procedure for coal mine drainage prediction (abs.). Geological Society of America, GSA Abstracts with Programs38, abstract 111241.

Hanor, J.S., 1968. Frequency distribution of compositions in the barite–celestite series. Am. Mineral 53, 1215–1222.

Hanshaw, B.B., Back, W., 1979. Major geochemical processes in the evolution of carbonate-aquifer systems. J. Hydrol. 43, 287–312.

Hedin, R.S., 2003. Recovery of marketable iron oxide from mine drainage in the USA. Land Contamin. Reclam. 11, 93–98.

Hedin, R.S., Nairn, R.W., Kleinmann, R.L.P., 1994. Passive treatment of coal mine drainage. U.S. Bureau of Mines Information Circular IC 9389.

Hedin, R.S., Stafford, S.L., Weaver, T.J., 2005. Acid mine drainage flowing from abandoned gas wells. Miner. Water Environ. 24, 104–106.

Hem, J.D., 1977. Reactions of metal ions at surfaces of hydrous iron oxide. Geochim. Cosmochim. Acta 41, 527–538.

Hem, J.D., 1978. Redox processes at surfaces of manganese oxide and their effects on aqueous metal ions. Chem. Geol. 21, 199–218.

Hem, J.D., 1985. Study and Interpretation of the Chemical Characteristics of Natural Waters, third ed. U.S. Geological Survey. Water-Supply Paper 2254.

Horowitz, A.J., Demas, C.R., Fitzgerald, K.K., Miller, T.L., Rickert, D.A., 1994. U.S. Geological Survey protocol for the collection and processing of surface-water samples for the subsequent determination of inorganic constituents in filtered water. U.S. Geological Survey. Open-File Rep. 94-539.

Houben, G., 2003. Iron oxide incrustations in wells, Part 1 – genesis, mineralogy and geochemistry. Appl. Geochem. 18, 927–939.

Hyman, D.M., Watzlaf, G.R., 1997. Metals and other components of coal mine drainage as related to aquatic life

standards. In: Proceedings of the 1997 National Meeting of the American Society for Surface Mining and Reclamation, May 10–15, 1997, Austin, Texas. American Society of Mining and Reclamation, pp. 531–545.

Kairies, C.L., Capo, R.C., Watzlaf, G.R., 2005. Chemical and physical properties of iron hydroxide precipitates associated with passively treated coal mine drainage in the Bituminous Region of Pennsylvania and Maryland. Appl. Geochem. 20, 1445–1460.

Kirby, C.S., Cravotta III, C.A., 2005a. Net alkalinity and net acidity. 1: Theoretical considerations. Appl. Geochem. 20, 1920–1940.

Kirby, C.S., Cravotta III, C.A., 2005b. Net alkalinity and net acidity. 2: Practical considerations. Appl. Geochem. 20, 1941–1964.

Kooner, Z.S., 1993. Comparative study of adsorption behavior of copper, lead, and zinc onto goethite in aqueous systems. Environ. Geol. 21, 250–342.

Langmuir, D., 1997. Aqueous Environmental Geochemistry. Prentice-Hall, New Jersey.

Loganathan, P., Burau, R.G., 1973. Sorption of heavy metal ions by a hydrous manganese oxide. Geochim. Cosmochim. Acta 37, 1277–1293.

Maree, J.P., Hlabela, P., Nengovhela, R., Geldenhuys, A.J., Mbhele, N., Nevhulaudzi, T., Waanders, F.B., 2004. Treatment of mine water for sulphate and metal removal using barium sulphide. Miner. Water Environ. 23, 195–203.

Mason, B., 1966. Principles of Geochemistry. John Wiley & Sons, New York.

McKenzie, R.M., 1980. The adsorption of lead and other heavy metals on oxides of manganese and iron. Aust. J. Soil Res. 18, 61–73.

Miller, S.D., 1980. Sulfur and hydrogen ion buffering in pyritic strip mine spoil. In: Trudinger, P.A., Walter, M.R. (Eds.), Biogeochemistry of Ancient and Modern Environments. Springer-Verlag, New York, pp. 537–543.

Morrison, J.L., Atkinson, S.D., Sheetz, B.E., 1990. Delineation of potential manganese sources in the coal overburdens of western Pennsylvania. In: Proceedings of the 1990 Mining and Reclamation Conference and Exhibition, Charleston, West Virginia, April 23–26, 1990, vol. 1. West Virginia University, Morgantown, West Virginia. pp. 249–256.

Mozley, P.S., 1989. Relationship between depositional environment and the elemental composition of early diagenetic siderite. Geology 17, 704–706.

Neal, C., Skeffington, R.A., Williams, R., Roberts, D.J., 1987. Aluminum solubility controls in acid waters – the need for a reappraisal: Earth Planet. Sci. Lett. 86, 105–112.

Nordstrom, D.K., 1977. Thermochemical redox equilibria of ZoBell's solution. Geochim. Cosmochim. Acta 41, 1835–1841.

Nordstrom, D.K., 2000. Advances in the hydrochemistry and microbiology of acid mine waters. Int. Geol. Rev. 42, 499–515.

Nordstrom, D.K., 2004. Modeling low-temperature geochemical processes. In: Drever, J.I. (Ed.), Surface and Ground Water Weathering, and Soils, Treatise on Geochemistry, vol. 5. Elsevier, pp. 37–72.

Nordstrom, D.K., Alpers, C.N., 1999. Geochemistry of acid mine waters. In, Plumlee, G.S., Logsdon, M.J. (Eds.), The Environmental Geochemistry of Mineral Deposits – Part A. Processes, Methods, and Health issues. Reviews in Economic Geology 6A, pp. 133–160.

Nordstrom, D.K., Ball, J.W., 1986. The geochemical behavior of aluminum in acidified surface waters. Science 232, 54–56.

Nordstrom, D.K., Jenne, E.A., Ball, J.W., 1979. Redox equilibria of iron in acid mine waters. In, Jenne, E.A. (Ed.), Chemical Modeling in Aqueous Systems – Speciation, Sorption, Solubility, and Kinetics. American Chemical Society of Symposium Series, vol. 93, pp. 51–79.

Nordstrom, D.K., Plummer, L.N., Langmuir, D., Busenberg, E., May, H.M., Jones, B.F., Parkhurst, D.L., 1990. Revised chemical equilibrium data for major water mineral reactions and their limitations. In: Melchior, D.C., Bassett, R.L. (Eds.), Chemical Modeling in Aqueous Systems II. American Chemical Society of Symposium Series, vol. 416, pp. 398–413.

Nordstrom, D.K., Alpers, C.N., Ptacek, C.J., Blowes, D.W., 2000. Negative pH and extremely acidic mine waters from Iron Mountain, California. Environ. Sci. Technol. 34, 254–258.

Nordstrom, D.K., Ball, J.W., McCleskey, R.B., 2006. Geochemistry of aluminum in surface and ground waters affected by acid rock drainage (abs.): Geological Society of America, GSA Abstracts with Programs, abstract 134-10.

Paces, T., 1973. Steady-state kinetics and equilibrium between ground water and granitic rock. Geochim. Cosmochim. Acta 37, 2541–2563.

Parkhurst, D.L., Appelo, C.A.J., 1999. User's guide to PHREEQC (Version 2) – a computer program for speciation, batch-reaction, one-dimensional transport, and inverse geochemical calculations: U.S. Geological Survey. Water Resource Invest. Rep. 99-4259. <http://wwwbrr.cr.usgs.gov/projects/GWC_coupled/phreeqci-2.11-148.exe> (accessed on the Word Wide Web on February 24, 2005).

Perry, E.F., 2001. Modelling rock-water interactions in flooded underground coal mines. Geochem. Explor. Environ. Anal. 1, 61–70.

Rantz, S.E. et al., 1982a. Measurement and computation of streamflow – 1. Measurement of stage and discharge. U.S. Geological Survey. Water-Supply Paper 2175.

Rantz, S.E. et al., 1982b. Measurement and computation of streamflow – 2. Computation of discharge. U.S. Geological Survey. Water-Supply Paper 2175.

Robbins, E.I., Nord, G.L., Savela, C.E., Eddy, J.I., Livi, K.J.T., Gullett, C.D., Nordstrom, D.K., Chou, I.-M., Briggs, K.M., 1996. Microbial and mineralogical analysis of aluminum-rich precipitates that occlude porosity in a failed anoxic limestone drain, Monongalia County, West Virginia. In: Chiang, Shiao-Hung (Ed.), Proceedings of the 13th Annual Internaternation Pittsburgh Coal Conference. Coal-Energy and the Environment, vol. 2. Reed & Witting Company, Pittsburgh, PA, pp. 761–767.

Robbins, E.I., Cravotta III, C.A., Savela, C.E., Nord Jr., G.L., 1999. Hydrobiogeochemical interactions in "anoxic" limestone drains for neutralization of acidic mine drainage. Fuel 78, 259–270.

Rose, A.W., Cravotta III, C.A., 1998. Geochemistry of coal-mine drainage. In: Brady, K.B.C., Smith, M.W., Schueck., J. (Eds.), Coal Mine Drainage Prediction and Pollution Prevention in Pennsylvania. Harrisburg, PA, Pennsylvania Department of Environmental Protection, 5600-BK-DEP2256, pp. 1.1–1.22.

Rose, S., Ghazi, A.M., 1997. Release of sorbed sulfate from iron oxyhydroxides precipitated from acid mine drainage

associated with coal mining. Environ. Sci. Technol. 31, 2136–2140.

Rose, A.W., Hawkes, H.E., Webb, J.S., 1979. Geochemistry in Mineral Exploration. Academic Press, New York.

Smedley, P.L., Kinniburgh, D.G., 2002. A review of the source, behaviour and distribution of arsenic in natural waters. Appl. Geochem. 17, 517–568.

Smith, K.S., Huyck, H.L.O., 1999. An overview of the abundance, relative mobility, bioavailability, and human toxicity of metals. In: Plumlee, G.S., Logsdon, M.J. (Eds.), The Environmental Geochemistry of Mineral Deposits – Part A. Processes, Methods, and Health Issues. Reviews in Economic Geology 6A, pp. 29–70.

Snoeyink, V.L., Jenkins, D., 1981. Water Chemistry. John Wiley & Sons Inc., New York.

Sparks, D.L., 2005. Toxic metals in the environment – the role of surfaces. Elements 1, 193–197.

Stumm, W., Morgan, J.J., 1996. Aquatic Chemistry – Chemical Equilibria and Rates in Natural Waters, third ed. John Wiley & Sons Inc., New York.

Thomas, R.C., Romanek, C.S., 2002. Passive treatment of low-pH, ferric dominated acid rock drainage in a vertical flow wetland – II. Metal removal. In: Proceedings of the 19th Annual Meeting of American Society of Mining and Reclamation, Lexington, Kentucky, June 9–13, 2002. American Society of Mining and Reclamation, pp. 752–775.

U.S. Environmental Protection Agency, 2000. Drinking water standards and health advisories (summer 2000). U.S. Environmental Protection Agency. <http://www.epa.gov/OST>.

U.S. Environmental Protection Agency, 2002a, National primary drinking water standards. U.S. Environmental Protection Agency EPA/816-F-02-013, July 2002. <http://www.epa.gov/safewater>.

U.S. Environmental Protection Agency, 2002b, National recommended water quality criteria–2002. U.S. Environmental Protection Agency EPA/822-R-02-047.

U.S. Geological Survey, variously dated, National field manual for the collection of water-quality data. U.S. Geological Survey. Tech. Water Resource Invest., Book 9, Chapters A1–A9, variously paged <http://pubs.water.usgs.gov/twri9A>.

Veizer, J., 1983. Trace elements and isotopes in sedimentary carbonates. In: Reeder, R.J. (Ed.), Carbonates – Mineralogy and Chemistry: Mineralogical Society of America Reviews in Mineralogy, vol. 11, pp. 265–299.

Webster, J.G., Swedlund, P.J., Webster, K.S., 1998. Trace metal adsorption onto an acid mine drainage iron(III) oxy hydroxy sulfate. Environ. Sci. Technol. 32, 1361–1368.

Whittemore, D.O., 1988. Bromide as a tracer in ground-water studies – Geochemistry and analytical determination. In: Proceedings of the Ground Water Geochemistry Conference, Dublin, OH, National Water Well Association, pp. 339–360.

Whittemore, D.O., Langmuir, D., 1975. The solubility of ferric oxyhydroxides in natural waters. Ground Water 13, 360–365.

Williams, D.J., Bigham, J.M., Cravotta III, C.A., Traina, S.J., Anderson, J.E., Lyon, G., 2002. Assessing mine drainage pH from the color and spectral reflectance of chemical precipitates. Appl. Geochem. 17, 1273–1286.

Winland, R.L., Traina, S.J., Bigham, J.M., 1991. Chemical composition of ochreous precipitates from Ohio coal mine drainage. J. Environ. Qual. 20, 452–460.

Wood, W.W., 1976. Guidelines for the collection and field analysis of ground-water samples for selected unstable constituents. U.S. Geological Survey. Tech. Water Resource Invest., Book 1, Chapter D2.

Yu, J.-Y., Heo, B., Choi, I.-K., Cho, J.-P., Change, H.-W., 1999. Apparent solubilities of schwertmannite and ferrihydrite in natural stream waters polluted by mine drainage. Geochim. Cosmochim. Acta 63, 3407–3416.

Yu, J.-Y., Park, M., Kim, J., 2002. Solubilities of synthetic schwertmannite and ferrihydrite. Geochem. J. 36, 119–132.

Table A1. Thermodynamic equilibrium constants at 25 °C used in constructing stability diagrams for mononuclear metal compounds and aqueous complexes[a]
[pK = -log(K) or -log(*B), where K and *B are equilibrium constants at 25 °C; n.a., not applicable]

Cation	Hydroxide Minerals[b]		Sulfate Minerals		Carbonate Minerals		Hydroxyl Species[c]				Chloride Species				Sulfate Species[d]			Carbonate Species[d]		
	pK^*_a	pK^*_c	pKa_{MSO4}	pKc_{MSO4}	pKa_{MCO3}	pKc_{MCO3}	p^*B_1	p^*B_2	p^*B_3	p^*B_4	pK_{1Cl}	pK_{2Cl}	pK_{3Cl}	pK_{4Cl}	pK_{1SO4}	pK_{2SO4}	pK_{HSO4}	pK_{1CO3}	pK_{2CO3}	pK_{HCO3}
Al^{3+}	-10.8	-8.11	3.23	-22.7	n.a.	n.a.	5.0	10.1	16.9	22.7	n.a.	n.a.	n.a.	n.a.	-3.02	-4.92	-0.46	n.a.	n.a.	n.a.
Ba^{2+}	n.a.	n.a.	9.97	n.a.	8.56	n.a.	13.47	n.a.	n.a.	n.a.	n.a.	n.a.	n.a.	n.a.	-2.70	n.a.	n.a.	-2.71	n.a.	-0.98
Ca^{2+}	-22.8	n.a.	4.36	4.58	8.34	8.48	12.78	n.a.	n.a.	n.a.	n.a.	n.a.	n.a.	n.a.	-2.30	n.a.	n.a.	-3.22	n.a.	-1.11
Cd^{2+}	-13.65	-13.73	1.873	0.10	12.1	n.a.	10.08	20.35	33.30	47.35	-1.98	-2.60	-2.40	n.a.	-2.46	-3.5	n.a.	-2.9	-6.4	-1.5
Co^{2+}	-13.1	n.a.	n.a.	n.a.	n.a.	n.a.	9.6	18.8	31.5	n.a.	n.a.	n.a.	n.a.	n.a.	n.a.	n.a.	n.a.	n.a.	n.a.	n.a.
Cu^{2+}	-8.64	-7.62	-3.01	2.64	9.63	n.a.	8.00	13.68	26.9	39.6	-0.43	-0.16	2.29	4.59	-2.31	n.a.	n.a.	-6.73	-9.83	-2.7
Fe^{2+}	-12.9	n.a.	2.21	n.a.	10.45	10.89	9.50	20.57	31.00	n.a.	-0.14	n.a.	n.a.	n.a.	-2.25	n.a.	-1.08	-4.38	n.a.	-2.0
Fe^{3+}	4.30	1.40	n.a.	n.a.	n.a.	n.a.	2.19	5.67	12.56	21.6	-1.48	-2.13	-1.13	n.a.	-4.04	-5.38	-2.48	n.a.	n.a.	n.a.
Mg^{2+}	-16.84	n.a.	2.14	n.a.	n.a.	n.a.	11.44	n.a.	n.a.	n.a.	n.a.	n.a.	n.a.	n.a.	-2.37	n.a.	n.a.	-2.98	n.a.	-1.07
Mn^{2+}	-15.2	n.a.	-2.67	n.a.	10.39	11.13	10.59	22.20	34.80	n.a.	-0.61	-0.25	0.31	n.a.	-2.25	n.a.	n.a.	-4.90	n.a.	-1.95
Ni^{2+}	-10.8	n.a.	2.04	2.36	6.84	n.a.	9.86	19.00	30.00	n.a.	-0.40	-0.96	n.a.	n.a.	-2.29	-1.02	n.a.	-6.87	-10.11	-2.14
Pb^{2+}	-8.15	n.a.	7.79	n.a.	13.13	n.a.	7.71	17.12	28.06	39.7	-1.60	-1.80	-1.70	-1.38	-2.75	-3.47	n.a.	-7.24	-10.64	-2.9
Sr^{2+}	n.a.	n.a.	6.63	n.a.	9.27	n.a.	13.29	n.a.	n.a.	n.a.	n.a.	n.a.	n.a.	n.a.	-2.29	n.a.	n.a.	-2.81	n.a.	-1.18
Zn^{2+}	-11.5	-12.45	1.96	-3.01	10	n.a.	8.96	16.9	28.4	41.2	-0.43	-0.45	-0.50	-0.20	-2.37	-3.28	n.a.	-5.3	-9.63	-2.1

a. Thermodynamic data from Ball and Nordstrom (1991), Nordstrom et al. (1990), Stumm and Morgan (1996), and Bigham et al. (1996).

b. Hydroxide mineral: pK* for $M(OH)_z + zH^+ = M^{z+} + zH_2O$ where z indicates charge on uncomplexed cation. Denoted with “a” for more soluble, amorphous phase and “c” for less soluble, crystalline phase.

c. For the general association reaction where “n” protonated ligands are added to “m” metal ions, speciation can be described as: $mM^{+z} + nHL = ML_n^{(z-n)} + nH^+$. For hydrolysis reactions, L = OH^-, and HL = H_2O. The overall equilibrium constant for this reaction can be written: $*B_n = \{M_mL_n^{(z-n)}\}\{H^+\}^n / \{M^{+z}\}^m\{HL\}^n$, where brackets denote activity of aqueous species. Rewriting and expressing as logarithm: $Log*B_n = Log\{M_mL_n^{(z-n)}\} - mLog\{M^{+z}\} - nLog\{HL\} - n(pH)$. See example computations for lead in Table A3.

d. Sulfate and carbonate species distributions as a function of pH are indicated by thermodynamic data for ligands in Table A2.

Table A2. Equilibrium reactions and corresponding mass-balance equations used to compute stabilities of aqueous lead species and solid lead compounds

[pK = -log(K) or -log(*B), where K and *B are equilibrium constants at 25 °C]

Equilibrium Reaction	Equilibrium Constant Equation	pK[a]	Expression for –Log Activity of Aqueous Complex
$Pb(OH)_2$ (s) + 2 H^+ = Pb^{2+} + 2 H_2O	$K_{Hydroxide} = \{Pb^{2+}\}/\{H^+\}^2$	-8.15	$p\{Pb^{2+}\} = pK_{Hydroxide} + 2\ pH$
$PbSO_4$ (s) = Pb^{2+} + SO_4^{2-}	$K_{Anglesite} = \{Pb^{2+}\}\{SO_4^{2-}\}$	7.79	$p\{Pb^{2+}\} = pK_{Anglesite} - p\{SO_4^{2-}\}$
$PbCO_3$ (s) = Pb^{2+} + CO_3^{2-}	$K_{Cerrusite} = \{Pb^{2+}\}\{CO_3^{2-}\}$	13.13	$p\{Pb^{2+}\} = pK_{Cerrusite} - p\{CO_3^{2-}\}$
Pb^{2+} + H_2O = $Pb(OH)^+$ + H^+	$*B_1 = \{Pb(OH)^+\}\{H^+\}/\{Pb^{2+}\}$	7.71	$p\{Pb(OH)^+\} = p*B_1 + p\{Pb^{2+}\} - pH$
Pb^{2+} + 2 H_2O = $Pb(OH)_2^0$ + 2 H^+	$*B_2 = \{Pb(OH)_2^0\}\{H^+\}^2/\{Pb^{2+}\}$	17.12	$p\{Pb(OH)_2^0\} = p*B_2 + p\{Pb^{2+}\} - 2\ pH$
Pb^{2+} + 3 H_2O = $Pb(OH)_3^-$ + 3 H^+	$*B_3 = \{Pb(OH)_3^-\}\{H^+\}^3/\{Pb^{2+}\}$	28.06	$p\{Pb(OH)_3^-\} = p*B_3 + p\{Pb^{2+}\} - 3\ pH$
Pb^{2+} + 4 H_2O = $Pb(OH)_4^{-2}$ + 4 H^+	$*B_4 = \{Pb(OH)_4^{-2}\}\{H^+\}^4/\{Pb^{2+}\}$	39.70	$p\{Pb(OH)_4^{-2}\} = p*B_4 + p\{Pb^{2+}\} - 4\ pH$
Pb^{2+} + Cl^- = $PbCl^+$	$K_{1Cl} = \{PbCl^+\}/(\{Pb^{2+}\}\{Cl^-\})$	-1.60	$p\{PbCl^+\} = pK_{1Cl} + p\{Pb^{2+}\} + p\{Cl^-\}$
Pb^{2+} + 2 Cl^- = $Pb(Cl)_2^0$	$K_{2Cl} = \{Pb(Cl)_2^0\}/(\{Pb^{2+}\}\{Cl^-\}^2)$	-1.80	$p\{Pb(Cl)_2^0\} = pK_{2Cl} + p\{Pb^{2+}\} + 2\ p\{Cl^-\}$
Pb^{2+} + 3 Cl^- = $Pb(Cl)_3^-$	$K_{3Cl} = \{Pb(Cl)_3^-\}/(\{Pb^{2+}\}\{Cl^-\}^3)$	-1.70	$p\{Pb(Cl)_3^-\} = pK_{3Cl} + p\{Pb^{2+}\} + 3\ p\{Cl^-\}$
Pb^{2+} + 4 Cl^- = $Pb(Cl)_4^{-2}$	$K_{4Cl} = \{Pb(Cl)_4^{-2}\}/(\{Pb^{2+}\}\{Cl^-\}^4)$	-1.38	$p\{Pb(Cl)_4^{-2}\} = pK_{4Cl} + p\{Pb^{2+}\} + 4\ p\{Cl^-\}$
Pb^{2+} + SO_4^{2-} = $PbSO_4^0$	$K_{1SO4} = \{PbSO_4^0\}/(\{Pb^{2+}\}\{SO_4^{2-}\})$	-2.75	$p\{PbSO_4^0\} = pK_{1SO4} + p\{Pb^{2+}\} + p\{SO_4^{2-}\}$
Pb^{2+} + 2 SO_4^{2-} = $Pb(SO_4)_2^{-2}$	$K_{2SO4} = \{Pb(SO_4)_2^{-2}\}/(\{Pb^{2+}\}\{SO_4^{2-}\}^2)$	-3.47	$p\{Pb(SO_4)_2^{-2}\} = pK_{2SO4} + p\{Pb^{2+}\} + 2\ p\{SO_4^{2-}\}$
Pb^{2+} + HCO_3^- = $PbHCO_3^+$	$K_{HCO3} = \{PbHCO_3^+\}/(\{Pb^{2+}\}\{HCO_3^-\})$	-2.90	$p\{PbHCO_3^+\} = pK_{HCO3} + p\{Pb^{2+}\} + p\{HCO_3^-\}$
Pb^{2+} + CO_3^{2-} = $PbCO_3^0$	$K_{1CO3} = \{PbCO_3^0\}/(\{Pb^{2+}\}\{CO_3^{2-}\})$	-7.24	$p\{PbCO_3^0\} = pK_{1CO3} + p\{Pb^{2+}\} + p\{CO_3^{2-}\}$
Pb^{2+} + 2 CO_3^{2-} = $Pb(CO_3)_2^{-2}$	$K_{2CO3} = \{Pb(CO_3)_2^{-2}\}/(\{Pb^{2+}\}\{CO_3^{2-}\}^2)$	-10.64	$p\{Pb(CO_3)_2^{-2}\} = pK_{2CO3} + p\{Pb^{2+}\} + 2\ p\{CO_3^{2-}\}$

Mass-Balance Expression[b]

$$[Pb_{TOT}] = [Pb^{2+}]+[Pb(OH)^+]+[Pb(OH)_2^0]+[Pb(OH)_3^-]+[Pb(OH)_4^{-2}]+[PbCl^-]+[PbCl_2^0]+[PbCl_3^-]+[PbCl_4^{-2}]+[PbSO_4^0]+[Pb(SO_4)_2^{-2}]+[PbHCO_3^+]+[PbCO_3^0]+[Pb(CO_3)_2^{-2}]$$

$$[Pb_{TOT}] = \{Pb^{2+}\}\,(1 + *B_1\{H^+\}^{-1} + *B_2\{H^+\}^{-2} + *B_3\{H^+\}^{-3} + *B_4\{H^+\}^{-4} + K_{1Cl}\{Cl^-\} + K_{2Cl}\{Cl^-\}^2 + K_{3Cl}\{Cl^-\}^3 + K_{4Cl}\{Cl^-\}^4 + K_{1SO4}\{SO_4^{2-}\} + K_{2SO4}\{SO_4^{2-}\}^2 + K_{HCO3}\{HCO_3^-\} + K_{1CO3}\{CO_3^{2-}\} + K_{2CO3}\{CO_3^{2-}\}^2)$$

a. Thermodynamic data from Ball and Nordstrom (1991).

b. Square brackets denote concentration; pointed brackets denote activity. Total activity equals sum of activities of individual species; total concentration can be estimated similarly by assuming activities equal concentrations (e.g. Drever, 1997, p. 200-203; Langmuir, 1997, p. 248-255). Precise estimate of concentration requires division of the activity of each aqueous specie by its activity coefficient.

Table A3. Equilibrium reactions and thermodynamic data used for construction of stability diagrams showing speciation and solubility relations for aluminum and iron[a]

[pK = -log(K), where K is equilibrium constant at 25 °C; n.a., not applicable]

Equilibrium Reaction	pK	Line Equation
Ligands:		
$H_2O = H^+ + OH^-$	14.0	$pH = pK - p\{OH^-\}$
$H_2SO_4 = H^+ + HSO_4^-$	-3.0	$pH = pK + p\{H_2SO_4\} - p\{HSO_4^-\}$
$HSO_4^- = H^+ + SO_4^{2-}$	1.99	$pH = pK + (p\{HSO_4^-\} - p\{SO_4^{2-}\}$
$H_2S = HS^- + H^+$	6.99	$pH = pK + (pH_2S\} - p\{HS^-\}$
$HS^- = S^{2-} + H^+$	12.92	$pH = pK + (p\{HS^-\} - p\{S^{2-}\}$
$H_2O + CO_2\ (gas) = H_2CO_3^*$	1.47	$p\{H_2CO_3^*\} = Pco_2 + pK$
$H_2CO_3^* = H^+ + HCO_3^-$	6.35	$pH = pK + p\{H_2CO_3^*\} - p\{HCO_3^-\}$
$HCO_3^- = H^+ + CO_3^{2-}$	10.33	$pH = pK + p\{HCO_3^-\} - p\{CO_3^{2-}\}$
Aluminum species:		
$Al^{3+} + H_2O = Al(OH)^{2+} + H^+$	5.0	$p\{Al(OH)^{2+}\} = pK + p\{Al^{3+}\} - pH$
$Al^{3+} + 2\ H_2O = Al(OH)_2^+ + 2\ H^+$	10.1	$p\{Al(OH)_2^+\} = pK + p\{Al^{3+}\} - 2\ pH$
$Al^{3+} + 3\ H_2O = Al(OH)_3^0 + 3\ H^+$	16.9	$p\{Al(OH)_3^0\} = pK + p\{Al^{3+}\} - 3\ pH$
$Al^{3+} + 4\ H_2O = Al(OH)_4^- + 4\ H^+$	22.7	$p\{Al(OH)_4^-\} = pK + p\{Al^{3+}\} - 4\ pH$
$Al^{3+} + HSO_4^- = AlHSO_4^{2+}$	-0.46	$p\{AlHSO_4^{2+}\} = pK - p\{Al^{3+}\} - p\{HSO_4^-\}$
$Al^{3+} + SO_4^{2-} = AlSO_4^+$	-3.02	$p\{AlSO_4^+\} = pK - p\{Al^{3+}\} - p\{SO_4^{2-}\}$
$Al^{3+} + 2\ SO_4^{2-} = Al(SO_4)_2^-$	-4.92	$p\{Al(SO_4)_2^-\} = pK - p\{Al^{3+}\} - 2\ p\{SO_4^{2-}\}$
Aluminum minerals:		
$Al(OH)_{3\ (Amorphous)}$: $Al(OH)_3 + 3\ H^+ = Al^{3+} + 3\ H_2O$	-10.8	$p\{Al^{3+}\} = pK + 3\ pH$
$Al(OH)_{3\ (Gibbsite)} + 3\ H^+ = Al^{3+} + 3\ H_2O$	-8.11	$p\{Al^{3+}\} = pK + 3\ pH$
$Al(SO_4)(OH)\cdot 5H_2O_{\ (Jurbanite)} + H^+ = Al^{3+} + SO_4^{2-} + 6\ H_2O$	3.3	$p\{Al^{3+}\} = pK - p\{SO_4^{2-}\} + pH$
$KAl_3(SO4)_2(OH)_{6\ (Alunite)} + 6\ H^+ = K^+ + 3\ Al^{3+} + 2\ SO_4^{2-} + 6\ H_2O$	1.4	$p\{Al^{3+}\} = {}^1/_3\ (pK - 2\ p\{SO_4^{2-}\} - p\{K^+\} + 6\ pH)$
$[Al(OH)_3]_{(1-x)}[SiO_2]_{(x)\ (Allophane)} + (3\text{-}3x)\ H^+ = (1\text{-}x)\ Al^{3+} + x\ H_4SiO_4^0 + (3\text{-}5x)\ H_2O$	K^b	$p\{Al^{3+}\} = {}^1/_{(1-x)}\ (pK - x\ p\{H_4SiO_4^0\}) + 3\ pH$
$Al_2Si_2O_5(OH)_{4\ (Kaolinite)} + 6\ H^+ = 2\ Al^{3+} + 2\ H_4SiO_4^0 + H_2O$	-7.44	$p\{Al^{3+}\} = {}^1/_2\ (pK - 2\ p\{H_4SiO_4^0\} + 6\ pH)$

(table continued on next page)

Table A3. Equilibrium reactions and thermodynamic data used for construction of stability diagrams showing speciation and solubility relations for aluminum and iron[a]

[pK = -log(K), where K is equilibrium constant at 25 °C; n.a., not applicable]

Equilibrium Reaction	pK	Line Equation
Ferrous species:		
$Fe^{2+} + H_2O = Fe(OH)^+ + H^+$	9.5	$p\{Fe(OH)^+\} = pK + p\{Fe^{2+}\} - pH$
$Fe^{2+} + 2\ H_2O = Fe(OH)_2^0 + 2\ H^+$	20.57	$p\{Fe(OH)_2^0\} = pK + p\{Fe^{2+}\} - 2\ pH$
$Fe^{2+} + 3\ H_2O = Fe(OH)_3^- + 3\ H^+$	31	$p\{Fe(OH)_3^-\} = pK + p\{Fe^{2+}\} - 3\ pH$
$Fe^{2+} + HSO_4^- = FeHSO_4^+$	-1.08	$p\{FeHSO_4^+\} = pK + p\{Fe^{2+}\} + p\{HSO_4^-\}$
$Fe^{2+} + SO_4^{2-} = FeSO_4^0$	-2.25	$p\{FeSO_4^0\} = pK + p\{Fe^{2+}\} + p\{SO_4^{2-}\}$
$Fe^{2+} + HCO_3^- = Fe(HCO_3)^+$	-2.0	$p\{Fe(HCO_3)^+\} = pK + p\{Fe^{2+}\} + p\{HCO_3^-\}$
Ferrous minerals:		
$Fe(OH)_{2\ (Amorphous)} + 2\ H^+ = Fe^{2+} + 2\ H_2O$	-12.9	$p\{Fe^{2+}\} = pK + 2pH$
$FeSO_4 \cdot 7H_2O_{\ (Melanterite)} = Fe^{2+} + SO_4^{2-} + 7\ H_2O$	2.21	$p\{Fe^{2+}\} = pK - p\{SO_4^{2-}\}$
$FeCO_{3\ (Siderite)} = Fe^{2+} + CO_3^{2-}$	10.89	$p\{Fe^{2+}\} = pK - p\{CO_3^{2-}\}$
Ferric species:		
$Fe^{3+} + H_2O = Fe(OH)^{2+} + H^+$	2.19	$p\{Fe(OH)^{2+}\} = pK + p\{Fe^{3+}\} - pH$
$Fe^{3+} + 2\ H_2O = Fe(OH)_2^+ + 2\ H^+$	5.67	$p\{Fe(OH)_2^+\} = pK + p\{Fe^{3+}\} - 2\ pH$
$Fe^{3+} + 3\ H_2O = Fe(OH)_3^0 + 3\ H^+$	12.56	$p\{Fe(OH)_3^0\} = pK + p\{Fe^{3+}\} - 3\ pH$
$Fe^{3+} + 4\ H_2O = Fe(OH)_4^- + 4\ H^+$	21.6	$p\{Fe(OH)_4^-\} = pK + p\{Fe^{3+}\} - 4\ pH$
$Fe^{3+} + HSO_4^- = FeHSO_4^{2+}$	-2.48	$p\{FeHSO_4^{2+}\} = pK - p\{Fe^{3+}\} - p\{HSO_4^-\}$
$Fe^{3+} + SO_4^{2-} = FeSO_4^+$	-4.04	$p\{FeSO_4^+\} = pK - p\{Fe^{3+}\} - p\{SO_4^{2-}\}$
$Fe^{3+} + 2\ SO_4^{2-} = Fe(SO_4)_2^-$	-5.38	$p\{Fe(SO_4)_2^-\} = pK - p\{Fe^{3+}\} - 2\ p\{SO_4^{2-}\}$
Ferric minerals:		
$Fe(OH)_{3\ (Ferrihydrite)} + 3\ H^+ = Fe^{3+} + 3H_2O$	-4.3	$p\{Fe^{3+}\} = pK + 3\ pH$
$FeOOH_{\ (Goethite)} + 3\ H^+ = Fe^{3+} + 2H_2O$	-1.4	$p\{Fe^{3+}\} = pK + 3\ pH$
$Fe_8O_8(OH)_{(8-2x)}(SO_4)_{x\ (Schwertmannite)} + (24-2x)\ H^+ = 8\ Fe^{3+} + x\ SO_4^{2-} + (16-2x)\ H_2O$	-18	$p\{Fe^{3+}\} = {}^1/_8\ (pK - x\ p\{SO_4^{2-}\} + (24-2x)\ pH)$
$KFe_3(SO_4)_2(OH)_{6\ (Jarosite)} + 6\ H^+ = K^+ + 3\ Fe^{3+} + 2\ SO_4^{2-} + 6\ H_2O$	12.51	$p\{Fe^{3+}\} = {}^1/_3\ (pK - 2\ p\{SO_4^{2-}\} - p\{K^+\} + 6\ pH)$

a. Thermodynamic predominance areas computed assuming constant $[SO_{4\ TOT}] = 10^{-1.68}$, $[CO_{3\ TOT}] = 10^{-2.0}$ to $10^{-5.0}$, $aK^+ = 10^{-4.3}$, and $aH_4SiO_4^0 = 10^{-3.76}$ and using thermodynamic data, listed above, compiled by Ball and Nordstrom (1991). Solubility data for goethite (FeOOH), ferrihydrite ($Fe(OH)_3$), schwertmannite ($Fe_8O_8(OH)_{(8-2x)}(SO_4)_x$), and jarosite ($KFe_3(SO_4)_2(OH)_6$) from Bigham et al. (1996). Schwertmannite stability computed assuming composition of $Fe_8O_8(OH)_{4.5}(SO_4)_{1.75}$ for sulfate content, x = 1.75.

b. Allophane stability computed for pK = (5.7 - 1.68·pH) and x = (1.24 - 0.135·pH) (Paces, 1973) and $aH_4SiO_4^0 = 10^{-3.52}$.